Conversion of the death inhibitor ARC to a killer activates pancreatic β-cell death in diabetes

Wendy M. McKimpson[1,2,5], **Yun Chen**[1,2,5], **James A. Irving**[8,9], **Min Zheng**[1,5], **Jeremy Weinberger**[1,2,5], **Wilson Lek Wen Tan**[10,11], **Zenia Tiang**[10,11], **Alistair M. Jagger**[8,9], **Streamson C. Chua Jr.**[1,3,6], **Jeffrey E. Pessin**[1,4,6], **Roger S.-Y. Foo**[10,11], **David A. Lomas**[8,9], **Richard N. Kitsis**[1,2,5,6,7,*]

[1]Department of Medicine, Albert Einstein College of Medicine, Bronx, NY 10461 USA

[2]Department of Cell Biology, Albert Einstein College of Medicine, Bronx, NY 10461 USA

[3]Department of Neuroscience, Albert Einstein College of Medicine, Bronx, NY 10461 USA

[4]Department of Molecular Pharmacology, Albert Einstein College of Medicine, Bronx, NY 10461 USA

[5]Department of Wilf Family Cardiovascular Research Institute, Albert Einstein College of Medicine, Bronx, NY 10461 USA

[6]Department of Einstein-Mount Sinai Diabetes Research Center, Albert Einstein College of Medicine, Bronx, NY 10461 USA

[7]Albert Einstein Cancer Center, Albert Einstein College of Medicine, Bronx, NY 10461 USA

[8]UCL Respiratory Medicine, University College London, London WC1E 6BN UK University College London

[9]Institute of Structural and Molecular Biology/Birkbeck, University of London, London WC1E 7HX UK

[10]Cardiovascular Research Institute, National University Health Systems, Singapore

[11]Genome Institute of Singapore, Agency for Science, Technology and Research, Singapore

SUMMARY

Loss of insulin-secreting pancreatic β-cells through apoptosis contributes to the progression of type 2 diabetes, but underlying mechanisms remain elusive. Here we identify a pathway in which

---

*Correspondence and Lead contact: Richard N. Kitsis, Albert Einstein College of Medicine, 1300 Morris Park Avenue, Bronx, NY 10461, Telephone (718) 430-2609, FAX (718) 430-8989, richard.kitsis@einstein.yu.edu.

DECLARATIONS OF INTERESTS

David Lomas is an inventor on the patent PCT/GB2019/051761 for a small molecule treatment of antitrypsin deficiency. This small molecule has not been used in this work.

the cell death inhibitor ARC paradoxically becomes a killer during diabetes. While cytoplasmic ARC maintains β-cell viability and pancreatic architecture, a pool of ARC relocates to the nucleus to induce β-cell apoptosis in humans with diabetes and several pathophysiologically-distinct mouse models. β-cell death results through the coordinate downregulation of serpins (serine protease inhibitors) not previously known to be synthesized and secreted by β-cells. Loss of the serpin α_1-antitrypsin from the extracellular space unleashes elastase, triggering the disruption of β-cell anchorage and subsequent cell death. Administration of α_1-antitrypsin to mice with diabetes prevents β-cell death and metabolic abnormalities. These data uncover a pathway for β-cell loss in type 2 diabetes and identify an FDA-approved drug that may impede progression of this syndrome.

eTOC Blurb

While cytoplasmic ARC maintains survival of insulin-producing pancreatic β-cells, McKimpson et al. show that a pool of ARC relocates to the nucleus during diabetes where it paradoxically triggers cell death. The mechanism involves downregulation of AAT expression and secretion unleashing elastase-dependent loss of β-cell adhesion and cell death.

Graphical Abstract
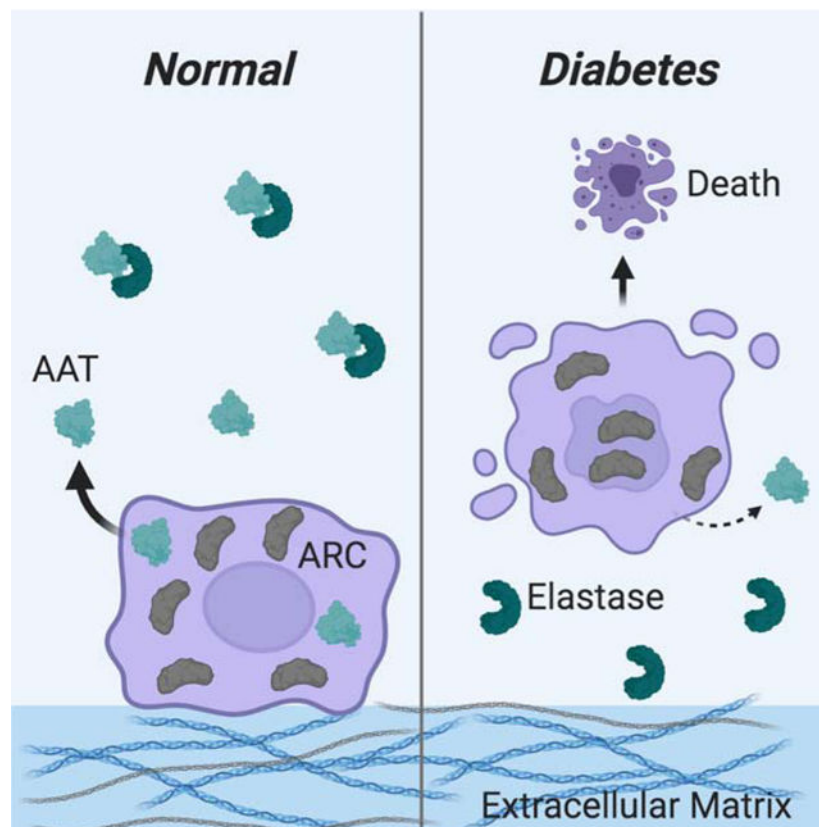
Keywords

diabetes; cell death; ARC; serpins; alpha-1 antitrypsin

INTRODUCTION

Type 2 diabetes, a syndrome associated with obesity, is characterized by elevated concentrations of glucose in the blood (hyperglycemia) that damage multiple organs including blood vessels, heart, kidneys, eyes, and the nervous system (Harcourt et al., 2013). Hyperglycemia develops initially because of insulin resistance, which is mediated by defective signaling at, or downstream of, the insulin receptor (Boucher et al., 2014). This impairs the uptake of circulating glucose and its metabolism in hepatocytes, adipocytes, and skeletal myocytes (Beck-Nielsen and Groop, 1994; Kahn, 1994). Development of the full syndrome, however, requires a second pathophysiological process termed β-cell failure. This is characterized by inadequate production and/or secretion of insulin from pancreatic β-cells, which results from their dysfunction or loss (Rhodes, 2005; Weir and Bonner-Weir, 2004). β-cell loss, in turn, occurs through dedifferentiation or cell death (Accili et al., 2016; Pick et al., 1998).

While at least a dozen cell death programs have been described (Galluzzi et al., 2018), β-cell death during type 2 diabetes occurs primarily by apoptosis. Apoptosis is mediated by two central pathways, an extrinsic pathway initiated by cell surface death receptors and an intrinsic pathway involving the mitochondria and endoplasmic reticulum (ER) (Danial and Korsmeyer, 2004; Del Re et al., 2019; Tait and Green, 2010). Both pathways lead to the activation of a hierarchy of caspases, which are cysteine proteases that cleave following aspartic acid residues within specific motifs (Pop and Salvesen, 2009). Genetic manipulations in the mouse indicate that both extrinsic and intrinsic apoptosis pathways are important in the pathogenesis of type 2 diabetes. For example, inhibition of the extrinsic pathway through β-cell-specific deletion of caspase-8 or inhibition of the intrinsic pathway through overexpression of the anti-cell death protein BCL-xL each protect against diabetes (Liadis et al., 2007; Zhou et al., 2000). Despite these genetic data, the signaling events responsible for killing β-cells during diabetes are poorly understood.

Apoptosis pathways are under negative, as well as positive, control. While most endogenous inhibitors of apoptosis antagonize either the extrinsic or intrinsic pathways, ARC (Apoptosis Repressor with Caspase recruitment domain (Geertman et al., 1996; Koseki et al., 1998); not to be confused with Activity-Regulated Cytoskeleton-associated protein) blocks both (Nam et al., 2004). ARC inhibits the extrinsic pathway by disrupting a multiprotein complex required for death receptor signaling (Nam et al., 2004). ARC inhibits the intrinsic pathway by binding to the pro-cell death protein BAX, abrogating BAX conformational activation and translocation to mitochondria (Gustafsson et al., 2004; Nam et al., 2004). Additionally, in some cell types, ARC binds p53 in the nucleus to inhibit p53 transcriptional activity and promote its nuclear export, thereby decreasing the transcription of cell death genes (Foo et al., 2007b). ARC is transcribed from the *NOL3* locus (Geertman et al., 1996; Koseki et al., 1998), which also gives rise to an alternatively spliced transcript NOP30 encoding a putative nucleolar protein (Stoss et al., 1999) (Figure S1). In contrast to the transcript encoding ARC, NOP30 mRNA is not conserved across mammalian species.

While the expression of ARC was initially thought to be restricted to cardiac and skeletal myocytes and some neuronal populations (Geertman et al., 1996; Koseki et al., 1998), we

observed that ARC is abundant in the endocrine, but not the exocrine, pancreas (McKimpson et al., 2013; McKimpson et al., 2017). In the endocrine pancreas (islets), ARC is most prominently expressed in insulin-secreting β-cells, although it is also present in other cell types at lower frequencies. ARC promotes β-cell survival and maintains pancreatic architecture during type 2 diabetes by inhibiting induction of the ER stress protein CHOP (McKimpson et al., 2013; McKimpson et al., 2017). Additionally, ARC may also act through inhibiting c-Jun N-terminal kinase signaling (Templin et al., 2017).

Alterations in ARC abundance have been shown to contribute to disease. For example, ARC is induced in multiple cancers where it promotes tumor growth, metastasis, and chemoresistance (McKimpson et al., 2015; Medina-Ramirez et al., 2011; Mercier et al., 2008; Mercier et al., 2005; Wang et al., 2005). Conversely, ARC abundance decreases in the heart and brain during ischemic injury mediated in some instances by degradation in the proteosome (Foo et al., 2007a; Hong et al., 2003; Nam et al., 2007). In contrast, ARC protein levels in β-cells remain constant during type 2 diabetes (McKimpson et al., 2013). This begs the question as to whether another mechanism regulates the actions of ARC in this syndrome. Herein we report the unexpected finding that a portion of ARC relocates from the cytoplasm to the the nucleus of β-cells during type 2 diabetes in humans and mice to activate a cell death pathway.

RESULTS

ARC in β-cells Translocates to the Nucleus During Diabetes

ARC is present in both the cytoplasm and nucleus of various normal and transformed cell types (Mercier et al., 2005; Wang et al., 2005). Our initial observations of immunostained pancreatic tissue from wild type mice suggested, however, that ARC resides exclusively in the cytoplasm of islet cells (McKimpson et al., 2013). Upon closer examination, however, we realized that ~20% of these cells in wild type mice contained nuclear ARC as demonstrated by co-localization with the nuclear marker DAPI (Figures 1A and 1B). In striking contrast, nuclear ARC was present in ~60% of islet cells in several mouse models of diabetes (Figures 1A and 1B). This was observed in pathophysiologically distinct models including *ob/ob* mice (which are deficient in leptin (Coleman and Hummel, 1973; Zhang et al., 1994)) and *Ins2* Akita/+ mice (in which a missense mutation in insulin causes misfolding and ER stress-induced apoptosis (Wang et al., 1999; Yoshioka et al., 1997)). The percentage of islet cells with nuclear ARC increased with age and duration of diabetes in *ob/ob* mice (Figure 1C). Importantly, staining was absent in islets from mice genetically lacking ARC (Figure 1D). Nuclear ARC was also found in pancreatic sections from *db/db* mice, a third model of diabetes characterized by a deficiency of the leptin receptor (Chua et al., 1996; Coleman, 1978; Lee et al., 1996) (Figure 1E), which was confirmed by subcellular fractionation of isolated pancreatic islets (Figure 1F). Similar results were observed in human pancreatic tissue specimens from controls and patients with type 2 diabetes (Figure 1G and Table S1). Consistent with our previous analyses of cytoplasmic ARC (McKimpson et al., 2013), much of the nuclear ARC (indicated by overlap of ARC and DAPI) resides in β-cells (indicated by insulin staining) (Figures 1H, 1I and S2). These data demonstrate that,

while total levels of ARC in islets remain constant (McKimpson et al., 2013), a portion of ARC translocates to the nucleus during diabetes.

Nuclear ARC Promotes Cell Death

To determine the functional consequences of nuclear-localized ARC, we created ARC constructs that were constitutively localized to either the nucleus (ARC-NLS) or cytoplasm (ARC-NES). For each of these constructs, we fused the localization sequence and a Myc tag to human ARC, which is functionally active in mouse cells (McKimpson et al., 2013), allowing us to distinguish the encoded protein from endogenous ARC. When these constructs were expressed at similar levels in MIN6 cells, a mouse β-cell line, we confirmed that ~85% of ARC-NLS was nuclear and ~100% of ARC-NES was cytoplasmic (Figures 2A–2C). ER stress is an important driver of β-cell apoptosis (Papa, 2012; Tabas and Ron, 2011). As anticipated, ARC-NES inhibited cell death elicited by ER stressors thapsigargin (which inhibits the sarco-endoplasmic reticulum Ca^{2+} ATPase) and the fatty acid palmitate (an ER stressor of clinical relevance to type 2 diabetes) (Figures 2D and 2F-2I, and S3). A similar trend was seen with tunicamycin (an inhibitor of N-linked glycosylation) (Figure 2E). In contrast, ARC-NLS paradoxically exacerbated cell death in response to each of these stimuli. Similar results were observed in U2OS osteosarcoma cells, which lack endogenous ARC (Foo et al., 2007b) (Figures 2J and 2K). These data demonstrate that, in contrast to the protective actions of cytoplasmic ARC, nuclear ARC promotes β-cell death.

Nuclear ARC Kills β-cells by Downregulating Serpin Expression

In β-cells, ARC protects cells from ER-stress induced apoptosis by preventing upregulation of the transcription factor CHOP, which becomes abundant during prolonged ER stress (McKimpson et al., 2013; McKimpson et al., 2017). While we observed that cytoplasmic ARC blunted upregulation of CHOP mRNA in response to thapsigargin as expected, overexpression of ARC in the nucleus did not significantly affect CHOP expression (Figure S4). These data suggested that cell death resulting from nuclear ARC involves another pathway.

To identify potential mechanisms by which nuclear ARC kills β-cells, we used RNA-seq to assess the transcriptome of MIN6 cells stably transfected with empty vector or ARC-NLS. Among other changes, cells expressing ARC-NLS exhibited a striking coordinate downregulation in the abundance of multiple transcripts encoding serpins (serine protease inhibitors) (Figure 3A). These included *serpina1a*, *a1b*, *a1c*, *a1d*, and *a1e*, which are genetic paralogs in the mouse that encode mRNAs differing in only untranslated regions. Each of these transcripts is translated to produce α_1-antitrypsin (AAT). Another downregulated serpin gene was *serpina3n*, which encodes α_1-antichymotrypsin. We confirmed RNA-seq changes in the multiple genes encoding AAT using qRT-PCR. These data showed that the levels of *serpina1a*, *a1b*, *a1c*, *a1d*, and *a1e* transcripts were decreased in MIN6 cells expressing ARC-NLS, but not ARC-NES (Figures 3B and 3C). Next, RNA interference was used to deplete *serpina1a*, *a1b*, and *a1c* transcripts in wild type MIN6 cells (Figure 3D). This exacerbated ER stress-induced cell death (Figure 3E), phenocopying the effect of nuclear ARC (Figure 2D).

AAT is a secreted protein synthesized primarily by the liver (Lucas et al., 2018). β-cells were not previously known to synthesize or secrete this protein. Measurement of AAT concentrations in MIN6 cells and corresponding media showed, however, that these cells synthesize AAT, ~80% of which is secreted (compare Figures 3D versus 3F). In parallel with the transcriptional downregulation of *serpina1* mRNAs by ARC-NLS (Figure 3B), AAT secretion also decreased by ~40% (Figures 3G).

To test whether decreases in secreted AAT are responsible for ER stress-induced cell death resulting from ARC-NLS, we added purified AAT (Figures 4A) to the media. Cell death was inhibited in a concentration-dependent manner (Figures 4B and 4C). Additionally, the protease inhibitory activity of AAT was required to reverse the increase in cell death resulting from ARC-NLS as inactive AAT (in which the reactive loop had been cleaved) was ineffective (Figures 4A and 4D). Further, these effects were independent of whether the cell culture media included serum, which we tested because serum might contain proteases that are targets of AAT inhibition (Figure 4E).

We also assessed the ability of the actual concentrations of AAT secreted by MIN6 cells to inhibit cell death using conditioned media. Media from cells transfected with empty vector (and, therefore, containing concentrations of AAT normally secreted by MIN6 cells) was compared with media from cells expressing ARC-NLS (containing decreased concentrations of secreted AAT; Figure 3G). When applied to ARC-NLS cells, media conditioned by empty vector cells was able to rescue ER stress-induced cell death back to baseline, while media conditioned by ARC-NLS cells was not able to do this (Figure 4F and S5). Taken together, these data indicate that nuclear translocation of ARC augments cell death by decreasing the amount of secreted AAT.

Restoration of serpin levels protects β-cells and alleviates diabetes in mice

To determine whether decreases in AAT abundance are also found in human diabetes, we immunostained pancreatic tissue from normal controls and patients with type 2 diabetes. AAT was observed in islets but not in the surrounding exocrine pancreas, and its abundance decreased markedly with type 2 diabetes (Figure 5A and Table S1). Levels of AAT transcripts were also decreased in islets isolated from *db/db* mice (Figure 5B). Further, less AAT was secreted from islets isolated from *ob/ob* mice (Figure 5C). We next determined if replacement of AAT could rescue β-cell death triggered by the free fatty acid palmitate, a physiologic stimuli relevant to diabetes. Pretreatment of islets isolated from wild type and *ob/ob* mice with AAT decreased ER-stress induced death as measured by TUNEL staining (Figures 5D and 5E). To test whether decreases in AAT contribute to β-cell death and metabolic abnormalities during diabetes *in vivo*, we administered AAT systemically to *ob/ob* mice over 14 weeks. This treatment markedly preserved islet area (Figure 5F) and reduced β-cell death (Figures 5G and 5H, Figure S6) with minimal changes to β-cell proliferation (Figure 5I). Administration of AAT to *ob/ob* mice also attenuated hyperglycemia (Figure 5J), and improved glucose tolerance (Figure 5K and 5L), while not affecting body weight (Figure S7).

Loss of serpins unleashes elastase-mediated disruption of cell adhesion

We next addressed the mechanism by which decreased AAT secretion induces β-cell death. Pathway analysis of the RNA-seq data indicated that cell adhesion was among the cellular processes most affected by nuclear ARC (Figure 6A). To explore a possible role for disruption of cell anchorage in β-cell death, we first assessed the effect of nuclear ARC on the numbers of cells that remain adherent to standard, uncoated tissue culture dishes under basal conditions (i.e. no death stimulus) 24 h after plating. Significantly fewer ARC-NLS cells remained attached compared with those transfected with empty vector (Figure 6B). Similar results were obtained with plates coated with fibronectin and laminin, key components of the vascular basement membrane and extracellular matrix in islets *in vivo* thought to be important in cellular function and survival (Nikolova et al., 2006; Stendahl et al., 2009) (Figure 6C). Decreases in cell adhesion due to ARC-NLS could not be explained by changes in baseline levels of cell death or proliferation as these parameters did not change over the time frame of these assays (Figures 6D and 6E). Furthermore, decreased adherence of ARC-NLS cells was not rescued by pre-treatment with the pan-caspase inhibitor z-VADfmk at concentrations sufficient to inhibit apoptosis (Figures 6F and 6G). These data suggest that nuclear ARC decreases cell adhesion upstream of effects on cell death.

To test whether decreases in extracellular serpins were responsible for the loss of cell adhesion, we used siRNA to reduce secreted AAT in wild type cells (Figure 3F), and found decreased adherence to tissue culture plates (Figure 7A) similar to that resulting from ARC-NLS (Figures 6B and 6C). Further, the use of conditioned media demonstrated that the concentrations of AAT normally secreted from control cells were sufficient to rescue adherence of ARC-NLS cells (Figures 7B and S5). Addition of purified AAT to the media also restored adherence of these cells and demonstrated that the anti-protease activity was required for this effect (Figure 7C).

The primary role of AAT is to inhibit elastase. Each of two elastase inhibitors blocked the increases in ER stress-induced cell death resulting from nuclear ARC, while inhibitors of trypsin, thrombin, and plasmin were ineffective (Figure 7D). Inhibition of elastase activity also prevented cell death in response to the physiologic stimulus palmitate in islets isolated from *ob/ob* mice (Figure 7E). Conversely, the addition of exogenous elastase to the cell culture media was itself sufficient to exacerbate ER stress-induced cell death in cells transfected with empty vector (Figure 7F). Further, inhibition of elastase restored adherence of ARC-NLS cells (Figure 7G). Taken together, these data indicate that increases in nuclear ARC promote downregulation of the expression and secretion of serpins resulting in elastase-dependent loss of cellular adhesion and subsequent β-cell death (Figure 7H).

DISCUSSION

This work reveals a molecular pathway that mediates β-cell death during type 2 diabetes. The essential elements are: (a) relocation of a pool of the cell death inhibitor ARC to the nucleus; (b) downregulation in the expression and secretion of AAT; (c) disinhibition of elastase in the extracellular space; (d) disruption of cell anchorage; and (e) and anoikis, a form of apoptosis induced by loss of cell anchorage (Frisch and Francis, 1994).

The percentage of pancreatic islet cells containing nuclear ARC is substantially higher in humans with type 2 diabetes and various genetic mouse models of this syndrome as compared with humans and mice without diabetes. As total islet ARC levels appear unaffected by diabetes (McKimpson et al., 2013), the increased presence of nuclear ARC suggests translocation of cytosolic ARC in the course of the syndrome. This raises the question as to whether β-cell death occurs from the loss of ARC in cytoplasm or the gain of ARC in the nucleus. While the former cannot be excluded as a contributing factor, several lines of evidence argue for activation of a death mechanism in the nucleus as the predominant mechanism. First, although the amounts of ARC that translocate to the nucleus in islets *in vivo* appear sufficient to decrease AAT expression, substantial levels of ARC remain in the cytoplasm. Second, while transfection of cytoplasm-localized ARC is protective as expected, transfection of nuclear-localized ARC activates cell death. Moreover, this is true in both β-cells that express endogenous ARC as well as in heterologous cells that do not. These observations provide direct evidence that nuclear ARC activates a death pathway. There is precedent for the general concept that the function of cell death regulators can be reversed. For example, caspase cleavage can convert anti-death proteins BCL-2 (Cheng et al., 1997) and BCL-xL (Clem et al., 1998) to killers. Here, relocation of ARC to the nucleus activates a killing mechanism that is distinct from the death mechanisms that ARC inhibits in the cytoplasm. The notion that nuclear ARC can induce a death program has been previously suggested, although a mechanism was not elucidated (Dowds and Sabban, 2001).

The machinery responsible for nuclear translocation of ARC is not clear as canonical NLS (or NES) motifs cannot be identified. It is possible that ARC moves to the nucleus in complex with another protein that contains a NLS, or that its relatively low molecular weight allows ARC to gain nuclear access independent of a NLS. Also unknown are the presumed molecular events that trigger nuclear translocation of ARC. Among others, these potentially include a post-translational modification of ARC or a change in its interactions with other proteins. It is notable that nuclear translocation of ARC is observed in mouse models of diabetes that differ in key respects. For example, *ob/ob* and *db/db* mice are obese, insulin resistant, and have high circulating insulin levels (Chua et al., 1996; Coleman, 1978; Zhang et al., 1994). In contrast, *Ins2* Akita/+ mice are lean, insulin sensitive, and have low circulating insulin levels (Wang et al., 1999; Yoshioka et al., 1997). A commonality among these models, however, is hyperglycemia. This raises the possibility that ARC may undergo enzymatic or non-enzymatic glycosylation which may be involved in its nuclear relocation. There is precedent for glycosylation promoting nuclear translocation of other proteins (Andrali et al., 2007; Erickson et al., 2013; Yang et al., 2008).

Nuclear ARC coordinately decreases the abundance of multiple serpin transcripts in β-cells. The mechanisms by which ARC modulates serpin expression, or whether this involves changes in gene transcription or mRNA stability, are unclear. ARC is composed of two domains: an N-terminal death-fold motif consisting of 5 anti-parallel α-helices (Jang et al., 2015) that mediates most of its protein-protein interactions; and an unstructured C-terminus containing proline-glutamic acid repeats whose function is unknown. Neither of these motifs has been previously implicated in transcription or mRNA stability. One possibility is that ARC interacts with proteins involved in one or both of these functions.

Loss and gain of function experiments support a causal connection between nuclear ARC-induced decreases in serpin AAT and β-cell death. First, AAT knockdown phenocopies the exacerbation of ER stress-induced cell death resulting from nuclear ARC. Second, addition of recombinant AAT to the media or conditioned media rescues the increment in ER stress-induced β-cell death resulting from transfected nuclear-localized ARC. Third, systemic administration of AAT rescues deaths of islet cells, hyperglycemia, and glucose intolerance in *ob/ob* mice *in vivo*.

During diabetes, β-cell loss can also occur by dedifferentiation as well as apoptosis. Our studies demonstrate a role for serpins in maintaining β-cell adhesion to promote cell survival. Whether serpins also play a role in β-cell dedifferentiation has yet to be determined. Interestingly, deletion of FOXO1 *in vivo*, which results in β-cell dedifferentiation (Talchai et al., 2012), also results in marked induction of *Serpina7* expression (Kim-Muller et al., 2016). Additional work will be needed to explore this possible connection between serpins and β-cell dedifferentiation.

Several lines of evidence converged to reveal the downstream events whereby nuclear ARC kills. First, AAT acting outside of the cell was able to rescue cell death. Second, rescue by AAT was proportionate to its concentration in the media. Third, AAT rendered defective for inhibiting serine proteases was unable to rescue. These data all point to a killing mechanism in which deficits in secreted AAT unleash the activity of a serine protease also outside of the cell, which is consistent with the pathway analysis of the RNA-seq data suggesting the involvement of cell adhesion processes. Analyses using inhibitors of serine proteases known to be inhibited by AAT showed that elastase – but not trypsin, plasmin, or thrombin – was necessary for ER stress-induced death in β-cells expressing nuclear-localized ARC. Cell death was blocked by two independent elastase inhibitors, and elastase itself was also sufficient to exacerbate cell death. Further elastase inhibition restored adhesion to β-cells transfected with nuclear-localized ARC. The relationship between cell adhesion and cell death is complex and bidirectional. Our observations suggest, however, that disruption of cell adhesion is primarily upstream of cell death in this pathway. This is evidenced by the fact that restoration of cell adhesion (with AAT or elastase inhibitors) rescued cell death, while direct inhibition of cell death with a pan-caspase inhibitor did not.

In our experiments, MIN6 cells expressing nuclear ARC had decreased cell adhesion to the ECM components laminin and fibronectin. This is interesting in light of recent data which suggests that β-cells may not deposit their own extracellular matrix, but instead attach to proteins deposited by the vascular basement membrane (Nikolova et al., 2006). This extracellular matrix produced by endothelial cells is rich in laminins, especially the isoforms laminin-411 and laminin-511; fibronectin is also found in these deposits (Geutskens et al., 2004; Otonkoski et al., 2008). Attachment of cells to the vascular basement membrane promotes β-cell proliferation and insulin secretion in mice and humans (Banerjee et al., 2012; Nikolova et al., 2006). Interestingly, recent evidence suggests that β-cells detach from the vascular membrane with diabetes (Kragl et al., 2016). Our data suggest that nuclear ARC could play a role in regulating this detachment.

The fact that β-cells and possibly other cells in islets express AAT was unexpected. AAT is known to be synthesized primarily by hepatocytes which secrete it into the circulation and, to a lesser extent, from monocytes/macrophages and lung and gut epithelial cells (Crystal, 1990; Janciauskiene et al., 2011). In comparison, the amounts synthesized by β-cells appear to be quite low. Islets are surrounded by a sea of exocrine pancreas that secrete multiple serine proteases into the pancreatic duct. In addition, β-cells themselves have been reported to secrete elastase, which may modulate insulin signaling (Esteghamat et al., 2019). We postulate that β-cells secrete AAT to protect themselves from these proteases. Interestingly, plasma AAT concentrations are 40–50% decreased in humans and mice with obesity and type 2 diabetes (Hashemi et al., 2007; Mansuy-Aubert et al., 2013; Sandstrom et al., 2008). While the extent to which decreased serum AAT levels contribute to reduced local levels surrounding β-cells is not clear, our cell culture and isolated islet studies indicate that the much lower levels from β-cells play an important role in regulating cell survival.

AAT is an approved therapy to oppose neutrophil elastase in individuals with genetic deficiency of AAT (Gadek et al., 1981; Wewers et al., 1987). It is also being considered as an anti-inflammatory in graft-versus-host disease, myocardial infarction, and type 1 diabetes, conditions in which inflammation is felt to be a major driver (Abouzaki et al., 2018; Ma et al., 2010; Magenau et al., 2018). The latter therapy is based on data that demonstrated AAT protected β-cells from death triggered by stressors associated with type 1 diabetes (Kalis et al., 2010; Koulmanda et al., 2012; Zhang et al., 2007). Similarly, new data supports that AAT may also protect islets from proinflammatory cytokines triggered by the aggregation of human islet amyloid polypeptide (Rodriguez-Comas et al., 2020). Our results suggest a mechanism and potential role for AAT in directly inhibiting β-cell death to stem the progression of type 2 diabetes, a distinct form of diabetes.

STAR Methods

RESOURCE AVAILABILITY

Lead Contact—Further information and requests for resources and reagents should be directed to and will be fulfilled by the Lead Contact, Dr. Richard Kitsis (richard.kitsis@einstein.yu.edu).

Materials Availability—All reagents generated for this paper are available upon request.

Data and Code Availability—RNA-seq data has been deposited in the SRA database (SRA accession: PRJNA563773) as is publically available at: https://www.ncbi.nlm.nih.gov/sra/PRJNA563773

EXPERIMENTAL MODEL AND SUBJECT DETAILS

Animal models—*ob/ob*, *db/db*, and *Ins2* Akita mice, each on a C57BL/6J background, were purchased from Jackson Laboratories (Bar Harbor, ME). In the case of *ob/ob* and *db/db* mice, heterozygote mutants were crossed to produce homozygote mutants and wild type littermates. For *Ins2* Akita mice, heterozygote mutant males were bred with wild type females to produce heterozygote mutants and wild type littermates. *Nol3* –/– mice on a

C57BL/6J background were generated and bred as previously described (Medina-Ramirez et al., 2011; Zaiman et al., 2011). Male mice were used for all experiments because they exhibit a more consistent diabetes phenotype. Ages and numbers of mice are as indicated in each figure. All studies were approved by the Institute for Animal Studies of the Albert Einstein College of Medicine.

Pancreatic Islets—Pancreatic islets were isolated from mice of the indicated genotypes as previous described (McKimpson et al., 2013). Briefly, a collagenase solution (1mg/mL; Roche) in M199 media (Gibco) was injected into the bile duct. Pancreata was subsequently removed and incubated at 37°C for 19 minutes. After several washes with M199 media, islets were separated from exocrine pancreas using Histopaque-1077 (Sigma-Aldrich), further purified by gravity sedimentation, and subsequently hand-picked under a microscope. Isolated islets were allowed to recover overnight in RPMI 1640 culture media supplemented with 10% fetal bovine serum (Gibco) and 1% penicillin streptomycin solution (Gibco). Islets of similar size were used for experiments. In order to get sufficient islets for analysis, each wild type sample represents islets pooled from three mice, and each *ob/ob* and *db/db* sample represents islets from a single mouse.

Human tissue—Human pancreatic tissue was obtained from the Network for Pancreatic Organ Donors with Diabetes (nPOD) tissue repository (Table S1). The human pancreatic tissue used in this study was from male individuals with or without type 2 diabetes. Specific age, duration of diabetes, and body mass index (BMI) is indicated in Table S1. These studies were in compliance with the Institutional Review Board of the Albert Einstein College of Medicine.

Cell lines—MIN6 pancreatic β-cells were a generous gift from Peter Arvan (University of Michigan) and cultured in DMEM with 4.5g/L glucose, L-glutamine, and sodium pyruvate (Sigma-Aldrich). Media was supplemented with 10% fetal bovine serum, 1% penicillin streptomycin solution, and 140 μmol/L β-mercaptoethanol (Sigma-Aldrich). U2OS osteosarcoma cells were purchased from ATCC and maintained in McCoy's 5a Medium Modified (ATCC) supplemented with 10% fetal bovine serum and 1% penicillin streptomycin solution.

METHOD DETAILS

AAT treatment and metabolic characterization of mice—Thirty 9 week-old male *ob/ob* mice were assigned to two groups of 15 each randomly except for the criteria that the mean body weights (Figure S7) and blood glucose concentrations were similar (Figure 5J). One group was randomly selected to receive AAT (PROLASTIN-C (Grifols)) dissolved in water (2 mg/mouse as a 40 μL intraperitoneal injection every three days (Ma et al., 2010)), while the other group received water alone (40 μL/mouse intraperitoneal injection every three days). Treatments were initiated at 9 weeks of age (before *ob/ob* mice exhibit abnormal glucose tolerance) and continued for 14 weeks. Four out of 15 mice in the AAT treatment group and 3 out of 15 in the water treatment group died over the course of the study. Body weights, blood glucose concentrations, and glucose tolerance tests were monitored as shown in the data. Blood glucose concentrations were measured using an OneTouch glucose

monitoring system (LifeScan) after an overnight fast. For glucose tolerance tests (GTT), mice were injected intraperitoneally with 1 g glucose/kg body weight (using 10% w/v D-glucose (Sigma-Aldrich)) after an overnight fast, following which blood glucose concentrations were measured at various time points. For each mouse, area under the curve (AUC) was calculated using the trapezoid rule at 0, 30, 60, 90, and 120 minutes after glucose injection.

Cell culture, plasmids, transfections—ARC-NLS, encoding human ARC followed by three copies of SV40 T-antigen NLS (DPKKKRKV) and then followed by a myc-tag, was generated by subcloning the ARC open reading frame into pShooter (Invitrogen) (Foo et al., 2007b). For ARC-NES, one copy of MAPKK NES (ALQKKLEELELDE) (Fukuda et al., 1997) was fused to the N-terminus of human ARC cDNA which was then followed by a myc-tag. This was generated by first attaching DNA sequences encoding the NES to the ARC opening reading frame using PCR and then subcloning this construct into pShooter (Invitrogen). The correctness of each construct was confirmed by DNA sequencing. *Serpina1* was knocked-down in MIN6 cells using Silencer Select siRNA targeted to mouse *serpina1a*, *a1b*, and *a1c* (s74223, Life Technologies).

For transient expression of plasmids and siRNA, cells were electroporated using Amaxa Cell Line Nucleofactor Kit V (Lonza) and studied 48 h later. Specifically 0.1 nmol Serpin siRNA or 4 μg ARC-NLS, ARC-NES or Vector plasmid was electroporated into MIN6 cells suspended in Solution V using Amaxa program G-016, and media replaced the next day. For U2OS cells, transient expression of plasmids was completed using Lipofectamine 3000 Reagent (Thermo Fisher) as recommended by the manufacturer and studied 48 h later. Stable MIN6 cell lines were generated by neomycin selection (using G418 (Geneticin, Thermo Fisher) at 750 μg/mL) after electroporation. Populations, not single clones, were studied in the case of stable transfectants.

Immunoblotting—Methods for cultured cells and isolated islets are as previously described (McKimpson et al., 2013). Gels were transferred onto nitrocellulose membranes and protein abundance detected with the following antibodies: ARC (Cayman Chemical), GAPDH (Abcam), PARP1 (Sigma-Aldrich), HMGA1 (Abcam), α-tubulin (Sigma-Aldrich), and secondary IRDye 800 and 680 antibodies (LI-COR). Immunoblot membranes were scanned using a LI-COR Odyssey and images quantified with ImageJ (National Institutes of Health).

Immunostaining—Methods for these procedures in cultured cells and pancreatic tissue are as previously described (McKimpson et al., 2013). Antibodies included ARC (Cayman Chemical), insulin (Abcam), insulin (Dako), cleaved caspase-3 (Cell Signaling Technology), pHistone H3 (Abcam), Myc-Tab (Cell Signaling), and AAT (provided by E. Miranda, Sapienza University of Rome and J. Perez, University of Malaga). Secondary antibodies included Alexa Fluor 488, 568, and 647 (Invitrogen) for immunostaining. Cover slips were applied using VECTASHIELD Mounting Medium with DAPI (Vector Laboratories) to counterstain nuclei. Images were collected with an Axio Observer.Z1 microscope (Zeiss). Confocal images were collected with a Zeiss LSM 510/710 confocal microscope (Zeiss).

Islet area measurements—Islet area was calculated by dividing total islet area by total pancreatic area for a single tissue section and then averaging islet area of adjacent sections. To accomplish this, H&E stained pancreatic sections were first scanned, and islet and total pancreas pixel area measured in ImageJ with the measure function.

AAT ELISA—Mouse *serpina1* (AAT) levels in conditioned media and cell lysates were measured by ELISA (Abnova) as recommended by the manufacturer. Prior to analysis, cells and islets were cultured in culture media for 24 h with no phenol red or FBS. For measurements in cells, lysates were harvested in PBS followed by sonication on ice. Relative values were normalized to protein standard provided with the kit.

Cell fractionation—For each sample, approximately 500 pancreatic islets were used. Following overnight recovery after isolation, primary islets were washed with PBS and exposed to trypsin for 1 minute at 37°C. Following deactivation of trypsin, cytoplasmic and nuclear fractions were prepared using NE-PER Nuclear and Cytoplasmic Extraction Reagent Kit (Thermo Fisher) as recommended by the manufacturer. Lysates were subsequently analyzed by immunoblot.

cDNA isolation and qRT-PCR—RNA and cDNA was generated as previously described (McKimpson and Accili, 2019). Briefly, RNA was isolated from cells and isolated islets using an Arcturus PicoPure RNA Isolation Kit (Applied Biosystems) as recommended by the manufacturer. The optional 15 minute DNaseI treatment step was included in this protocol. qScript cDNA SuperMix (Quanta Biosciences) was used as recommended to make cDNA. qPCR reactions were completed with the primers listed in the key resources table using GoTaq qPCR Master Mix (Promega). Measurements were made using a Bio-Rad CFX96 real-time PCR system, and relative gene expression levels were calculated using the Ct method with GAPDH as the reference gene.

Cell death assays—Cell death was induced with thapsigargin 1 μM (Fisher Scientific), tunicamycin 5 ng/mL (Sigma-Aldrich), or palmitate 1.2 mM (Sigma-Aldrich) in MIN6 cells and isolated islets. For palmitate treatment, sodium palmitate powder was freshly resuspended in culture media supplemented with 600 μM BSA and then dissolved by shaking overnight at 55°C. Media was filter sterilized prior to the experiment. Culture media supplemented with 600 μM BSA served as control. For MIN6 cells, cell death was assessed 24 h later using live/dead staining with propidium iodide (PI) or using TUNEL (Roche) as previously described (McKimpson et al., 2013). For isolated islets, cell death was assessed after 3 d treatment and assessed using TUNEL, which was performed on samples fixed in 4% PFA for 10 minutes rotating at 4°C, embedded in OCT, and sectioned prior to staining. Proteinase K treatment was omitted in TUNEL assays performed on MIN6 cells and isolated islets but included in assays performed on pancreatic tissue according to manufacturer's recommendation. To determine the % TUNEL positive β-cells, the analysis was restricted to insulin-positive cells. In experiments in which the effects of various inhibitors on cell death were tested, the inhibitor was added 2 h before the death inducer. Treatments included: z-VADfmk (pan-caspase inhibitor) 200 μM (R&D Systems), AAT 0.5 mg/mL unless specified otherwise (purified by the investigators as described below), *N*-methoxysuccinyl-Ala-Ala-

Pro-Val-chloromethyl ketone (elastase inhibitor) 0.2 mg/mL (Molecular Probes), elafin (elastase inhibitor) 0.1 mg/mL (Sigma-Aldrich), BPTI 10 µM (trypsin inhibitor) (Sigma-Aldrich), and the thrombin and plasmin inhibitors (both obtained from respective SensoLyte AFC kits by AnaSpec) used at 1:500 dilution of the supplied solution.

Preparation of Conditioned media—Conditioned media was prepared by culturing 3×10^6 of the indicated cells for 24 h in 4 ml media. The following day, media was cleared by centrifugation at 1000 x g for 3 min and then used as indicated undiluted.

Preparation of active and cleaved AAT—AAT was purified from wild-type (MM homozygote) human plasma by 1:3 dilution into PBS and application at 2 ml/min to 20 ml Alpha-1 Antitrypsin Select resin (GE Healthcare). After washing with PBS to baseline, bound protein was eluted with 2 M $MgCl_2$ in 20 mM Tris pH7.4, dialyzed 1:1000 against 20 mM Tris pH8.4 overnight, reduced with 50 mM β-mercaptoethanol for 10 min and applied to a 5 ml HiTrap Q Sepharose column (GE Healthcare). AAT was eluted using a 0 to 0.5 M NaCl gradient across 80 ml, with fractions selected based on homogeneity by SDS-PAGE and non-denaturing PAGE. Pooled material was buffer exchanged into PBS and stored at −80°C until use. For preparation of reactive center loop-cleaved (inactivated) AAT, the purified protein was diluted to 1 mg/ml and incubated for 18 hours at 37°C at a 50:1 molar excess over endoprotease GluC (Sigma Aldrich)(Lomas et al., 1995). A ~4 kDa difference in size by SDS-PAGE confirmed the reaction had run to completion. Protease was removed by re-purification using a HiTrap Q sepharose column as described above with a 0 to 1 M NaCl gradient. Successful inactivation was confirmed using a chymotrypsin inhibition assay as described (Irving et al., 2014).

Cell adherence assays—Cell adhesion to untreated tissue culture plates was assessed by plating 250,000 cells/well in a 12-well plate overnight, and then counting the number of cells following staining with Hoechst 33342 (Invitrogen). In experiments in which the effects of various treatments on cell adhesion was tested, the indicated treatment was added after overnight plating and the experiment continued for an additional 24 h. Cell adhesion to components of the extracellular matrix was measured using the CytoSelect 48-Well Cell Adhesion Assay ECM Array (Cell Biolabs). For these experiments, 150,000 cells/well were plated and allowed to adhere for 90 min under standard cell culture conditions. Cell number was determined colorimetrically with background adherence to BSA-coated wells subtracted from adherence to the various substrates.

QUANTIFICATION AND STATISTICAL ANALYSIS

RNA-seq and computation analysis—RNA-seq was performed on Illumina HiSeq4000. Paired-end reads were mapped against mouse genome (mm9) using Tophat version 2.0.11 with default parameters (Trapnell et al., 2012). Subsequently, gene expression was computed using Cufflinks version 2.2.1 using GENCODE version M1 reference GTF (Trapnell et al., 2012). Differential gene expression analysis was performed using Cuffdiff version 2.2.1 (Trapnell et al., 2012). Mapped reads were converted to bigwig format and were visualized on UCSC Genome Browser (Kent et al., 2002). Gene expression heatmap was generated using R (version 3.1.2). Pathway analysis was performed on differentially

expressed genes using Database for Annotation, Visualization and Integrated Discovery (DAVID http://david.abcc.ncifcrf.gov/) (Huang da et al., 2009).

Replication, randomization, and quantification

Replicates and display of data: The numbers of independent experiments are specified panel by panel in the figure legends. In the following panels, we display pooled data from independent experiments without any normalization: Figures 1B, 1C, 1F, 1G, 2G, 2H, 2I, 2K, 3B, 3C, 3D, 3E, 3F, 3G, 4B, 4C, 4D, 4E, 5A, 5B, 5C, 5D, 5E, 5F, 5G, 5H, 5I, 5J, 5K, 5L, 6B, 6C, 6D, 6E, 6F, 6G, 7A, 7C, 7E, 7F, 7G, S4, and S7. Where variability in the magnitude (but not directionality) of effects necessitated normalization in order to pool data, we displayed a representative experiment in the main figures: Figures 2D, 2E, 2F, 4F, and 7B. In these cases, normalized pooled data from independent experiments were shown in the supplemental figures: Figures S3, S5. For Figure 7D, 3 representative experiments are shown in that panel. The rationale for showing a representative experiment in these cases is to provide the reader with the absolute magnitude of the parameter being measured, which would not be apparent from normalized pooled data. *Technical replicates pertaining to micrographic analyses:* For cultured cells, 6 randomly chosen fields (~150–350 cells) were scored. For tissue, 20 randomly chosen islets per section were assessed. For the RNA-seq experiment, there were 3 technical replicates in each group.

Statistical analyses: For comparisons between two groups, a two-tailed student's t-test was performed. Multiple comparisons were analyzed using analysis of variance followed by a Tukey post-hoc test. GraphPad Prism 6 software (La Jolla, CA) was used for calculations. $P < 0.05$ was deemed significant.

Randomization: Mice were assigned to two groups randomly except for the criteria that the starting mean body weights and fasting blood glucose concentrations be equivalent between the groups. The groups were then randomly assigned to treatment with AAT in water or water alone. As described in detail above, survival among the two groups to study end was equivalent. For some of the post-mortem tissue analyses, specimens from every mouse were not studied. However, those studied were chosen randomly and equal numbers were studied for each treatment group.

Supplementary Material

Refer to Web version on PubMed Central for supplementary material.

ACKNOWLEDGEMENTS

REFERENCES

Abouzaki NA, Christopher S, Trankle C, Van Tassell BW, Carbone S, Mauro AG, Buckley L, Toldo S, and Abbate A. (2018). Inhibiting the Inflammatory Injury After Myocardial Ischemia Reperfusion With Plasma-Derived Alpha-1 Antitrypsin: A Post Hoc Analysis of the VCU-alpha1RT Study. J Cardiovasc Pharmacol 71, 375–379. [PubMed: 29634656]

Accili D, Talchai SC, Kim-Muller JY, Cinti F, Ishida E, Ordelheide AM, Kuo T, Fan J, and Son J. (2016). When beta-cells fail: lessons from dedifferentiation. Diabetes Obes Metab 18 Suppl 1, 117–122. [PubMed: 27615140]

Andrali SS, Qian Q, and Ozcan S. (2007). Glucose mediates the translocation of NeuroD1 by O-linked glycosylation. J Biol Chem 282, 15589–15596. [PubMed: 17403669]

Banerjee M, Virtanen I, Palgi J, Korsgren O, and Otonkoski T. (2012). Proliferation and plasticity of human beta cells on physiologically occurring laminin isoforms. Mol Cell Endocrinol 355, 78–86. [PubMed: 22314207]

Beck-Nielsen H, and Groop LC (1994). Metabolic and genetic characterization of prediabetic states. Sequence of events leading to non-insulin-dependent diabetes mellitus. J Clin Invest 94, 1714–1721. [PubMed: 7962519]

Boucher J, Kleinridders A, and Kahn CR (2014). Insulin receptor signaling in normal and insulin-resistant states. Cold Spring Harb Perspect Biol 6.

Cheng EH, Kirsch DG, Clem RJ, Ravi R, Kastan MB, Bedi A, Ueno K, and Hardwick JM (1997). Conversion of Bcl-2 to a Bax-like death effector by caspases. Science 278, 1966–1968. [PubMed: 9395403]

Chua SC Jr., Chung WK, Wu-Peng XS, Zhang Y, Liu SM, Tartaglia L, and Leibel RL (1996). Phenotypes of mouse diabetes and rat fatty due to mutations in the OB (leptin) receptor. Science 271, 994–996. [PubMed: 8584938]

Clem RJ, Cheng EH, Karp CL, Kirsch DG, Ueno K, Takahashi A, Kastan MB, Griffin DE, Earnshaw WC, Veliuona MA, et al. (1998). Modulation of cell death by Bcl-XL through caspase interaction. Proc Natl Acad Sci U S A 95, 554–559. [PubMed: 9435230]

Coleman DL (1978). Obese and diabetes: two mutant genes causing diabetes-obesity syndromes in mice. Diabetologia 14, 141–148. [PubMed: 350680]

Coleman DL, and Hummel KP (1973). The influence of genetic background on the expression of the obese (Ob) gene in the mouse. Diabetologia 9, 287–293. [PubMed: 4588246]

Crystal RG (1990). Alpha 1-antitrypsin deficiency, emphysema, and liver disease. Genetic basis and strategies for therapy. J Clin Invest 85, 1343–1352. [PubMed: 2185272]

Danial NN, and Korsmeyer SJ (2004). Cell death: critical control points. Cell 116, 205–219. [PubMed: 14744432]

Del Re DP, Amgalan D, Linkermann A, Liu Q, and Kitsis RN (2019). Fundamental Mechanisms of Regulated Cell Death and Implications for Heart Disease. Physiol Rev 99, 1765–1817. [PubMed: 31364924]

Dowds TA, and Sabban EL (2001). Endogenous and exogenous ARC in serum withdrawal mediated PC12 cell apoptosis: a new pro-apoptotic role for ARC. Cell Death Differ 8, 640–648. [PubMed: 11536015]

Erickson JR, Pereira L, Wang L, Han G, Ferguson A, Dao K, Copeland RJ, Despa F, Hart GW, Ripplinger CM, et al. (2013). Diabetic hyperglycaemia activates CaMKII and arrhythmias by O-linked glycosylation. Nature 502, 372–376. [PubMed: 24077098]

Esteghamat F, Broughton JS, Smith E, Cardone R, Tyagi T, Guerra M, Szabo A, Ugwu N, Mani MV, Azari B, et al. (2019). CELA2A mutations predispose to early-onset atherosclerosis and metabolic syndrome and affect plasma insulin and platelet activation. Nat Genet 51, 1233–1243. [PubMed: 31358993]

Foo RS, Chan LK, Kitsis RN, and Bennett MR (2007a). Ubiquitination and degradation of the anti-apoptotic protein ARC by MDM2. J Biol Chem 282, 5529–5535. [PubMed: 17142834]

Foo RS, Nam YJ, Ostreicher MJ, Metzl MD, Whelan RS, Peng CF, Ashton AW, Fu W, Mani K, Chin SF, et al. (2007b). Regulation of p53 tetramerization and nuclear export by ARC. Proc Natl Acad Sci U S A 104, 20826–20831. [PubMed: 18087040]

Frisch SM, and Francis H. (1994). Disruption of epithelial cell-matrix interactions induces apoptosis. J Cell Biol 124, 619–626. [PubMed: 8106557]

Fukuda M, Gotoh I, Adachi M, Gotoh Y, and Nishida E. (1997). A novel regulatory mechanism in the mitogen-activated protein (MAP) kinase cascade. Role of nuclear export signal of MAP kinase kinase. The Journal of biological chemistry 272, 32642–32648. [PubMed: 9405481]

Gadek JE, Klein HG, Holland PV, and Crystal RG (1981). Replacement therapy of alpha 1-antitrypsin deficiency. Reversal of protease-antiprotease imbalance within the alveolar structures of PiZ subjects. J Clin Invest 68, 1158–1165. [PubMed: 7028785]

Galluzzi L, Vitale I, Aaronson SA, Abrams JM, Adam D, Agostinis P, Alnemri ES, Altucci L, Amelio I, Andrews DW, et al. (2018). Molecular mechanisms of cell death: recommendations of the Nomenclature Committee on Cell Death 2018. Cell Death Differ 25, 486–541. [PubMed: 29362479]

Geertman R, McMahon A, and Sabban EL (1996). Cloning and characterization of cDNAs for novel proteins with glutamic acid-proline dipeptide tandem repeats. Biochim Biophys Acta 1306, 147–152. [PubMed: 8634331]

Geutskens SB, Homo-Delarche F, Pleau JM, Durant S, Drexhage HA, and Savino W. (2004). Extracellular matrix distribution and islet morphology in the early postnatal pancreas: anomalies in the non-obese diabetic mouse. Cell Tissue Res 318, 579–589. [PubMed: 15480796]

Gustafsson AB, Tsai JG, Logue SE, Crow MT, and Gottlieb RA (2004). Apoptosis repressor with caspase recruitment domain protects against cell death by interfering with Bax activation. J Biol Chem 279, 21233–21238. [PubMed: 15004034]

Harcourt BE, Penfold SA, and Forbes JM (2013). Coming full circle in diabetes mellitus: from complications to initiation. Nature reviews Endocrinology 9, 113–123.

Hashemi M, Naderi M, Rashidi H, and Ghavami S. (2007). Impaired activity of serum alpha-1-antitrypsin in diabetes mellitus. Diabetes Res Clin Pract 75, 246–248. [PubMed: 16875754]

Hong YM, Jo DG, Lee JY, Chang JW, Nam JH, Noh JY, Koh JY, and Jung YK (2003). Down-regulation of ARC contributes to vulnerability of hippocampal neurons to ischemia/hypoxia. FEBS Lett 543, 170–173. [PubMed: 12753927]

Huang da W, Sherman BT, and Lempicki RA (2009). Systematic and integrative analysis of large gene lists using DAVID bioinformatics resources. Nature protocols 4, 44–57. [PubMed: 19131956]

Irving JA, Haq I, Dickens JA, Faull SV, and Lomas DA (2014). Altered native stability is the dominant basis for susceptibility of alpha1-antitrypsin mutants to polymerization. The Biochemical journal 460, 103–115.

Janciauskiene SM, Bals R, Koczulla R, Vogelmeier C, Kohnlein T, and Welte T. (2011). The discovery of alpha1-antitrypsin and its role in health and disease. Respir Med 105, 1129–1139. [PubMed: 21367592]

Jang TH, Kim SH, Jeong JH, Kim S, Kim YG, and Park HH (2015). Crystal structure of caspase recruiting domain (CARD) of apoptosis repressor with CARD (ARC) and its implication in inhibition of apoptosis. Scientific reports 5, 9847. [PubMed: 26038885]

Kahn CR (1994). Banting Lecture. Insulin action, diabetogenes, and the cause of type II diabetes. Diabetes 43, 1066–1084. [PubMed: 8039601]

Kalis M, Kumar R, Janciauskiene S, Salehi A, and Cilio CM (2010). alpha 1-antitrypsin enhances insulin secretion and prevents cytokine-mediated apoptosis in pancreatic beta-cells. Islets 2, 185–189. [PubMed: 21099312]

Kent WJ, Sugnet CW, Furey TS, Roskin KM, Pringle TH, Zahler AM, and Haussler D. (2002). The human genome browser at UCSC. Genome research 12, 996–1006. [PubMed: 12045153]

Kim-Muller JY, Fan J, Kim YJ, Lee SA, Ishida E, Blaner WS, and Accili D. (2016). Aldehyde dehydrogenase 1a3 defines a subset of failing pancreatic beta cells in diabetic mice. Nat Commun 7, 12631. [PubMed: 27572106]

Koseki T, Inohara N, Chen S, and Nunez G. (1998). ARC, an inhibitor of apoptosis expressed in skeletal muscle and heart that interacts selectively with caspases. Proc Natl Acad Sci U S A 95, 5156–5160. [PubMed: 9560245]

Koulmanda M, Bhasin M, Fan Z, Hanidziar D, Goel N, Putheti P, Movahedi B, Libermann TA, and Strom TB (2012). Alpha 1-antitrypsin reduces inflammation and enhances mouse pancreatic islet transplant survival. Proc Natl Acad Sci U S A 109, 15443–15448. [PubMed: 22949661]

Kragl M, Schubert R, Karsjens H, Otter S, Bartosinska B, Jeruschke K, Weiss J, Chen C, Alsteens D, Kuss O, et al. (2016). The biomechanical properties of an epithelial tissue determine the location of its vasculature. Nat Commun 7, 13560. [PubMed: 27995929]

Kung G, McKimpson W, Kitsis RN (2010). NOL3 (nucleolar protein 3 (apoptosis repressor with CARD domain)) (Atlas Genet Cytogenet Oncol Haematol. 2010;14(4):400–403).

Lee GH, Proenca R, Montez JM, Carroll KM, Darvishzadeh JG, Lee JI, and Friedman JM (1996). Abnormal splicing of the leptin receptor in diabetic mice. Nature 379, 632–635. [PubMed: 8628397]

Liadis N, Salmena L, Kwan E, Tajmir P, Schroer SA, Radziszewska A, Li X, Sheu L, Eweida M, Xu S, et al. (2007). Distinct in vivo roles of caspase-8 in beta-cells in physiological and diabetes models. Diabetes 56, 2302–2311. [PubMed: 17563067]

Lomas DA, Elliott PR, Chang WS, Wardell MR, and Carrell RW (1995). Preparation and characterization of latent alpha 1-antitrypsin. The Journal of biological chemistry 270, 5282–5288. [PubMed: 7890640]

Lucas A, Yaron JR, Zhang L, and Ambadapadi S. (2018). Overview of Serpins and Their Roles in Biological Systems. Methods Mol Biol 1826, 1–7. [PubMed: 30194590]

Ma H, Lu Y, Li H, Campbell-Thompson M, Parker M, Wasserfall C, Haller M, Brantly M, Schatz D, Atkinson M, et al. (2010). Intradermal alpha1-antitrypsin therapy avoids fatal anaphylaxis, prevents type 1 diabetes and reverses hyperglycaemia in the NOD mouse model of the disease. Diabetologia 53, 2198–2204. [PubMed: 20593162]

Magenau JM, Goldstein SC, Peltier D, Soiffer RJ, Braun T, Pawarode A, Riwes MM, Kennel M, Antin JH, Cutler CS, et al. (2018). alpha1-Antitrypsin infusion for treatment of steroid-resistant acute graft-versus-host disease. Blood 131, 1372–1379. [PubMed: 29437593]

Mansuy-Aubert V, Zhou QL, Xie X, Gong Z, Huang JY, Khan AR, Aubert G, Candelaria K, Thomas S, Shin DJ, et al. (2013). Imbalance between neutrophil elastase and its inhibitor alpha1-antitrypsin in obesity alters insulin sensitivity, inflammation, and energy expenditure. Cell Metab 17, 534–548. [PubMed: 23562077]

McKimpson WM, and Accili D. (2019). A fluorescent reporter assay of differential gene expression response to insulin in hepatocytes. Am J Physiol Cell Physiol 317, C143–C151. [PubMed: 31091147]

McKimpson WM, Weinberger J, Czerski L, Zheng M, Crow MT, Pessin JE, Chua SC Jr., and Kitsis RN (2013). The apoptosis inhibitor ARC alleviates the ER stress response to promote beta-cell survival. Diabetes 62, 183–193. [PubMed: 22933109]

McKimpson WM, Yuan Z, Zheng M, Crabtree JS, Libutti SK, and Kitsis RN (2015). The Cell Death Inhibitor ARC Is Induced in a Tissue-Specific Manner by Deletion of the Tumor Suppressor Gene Men1, but Not Required for Tumor Development and Growth. PLoS One 10, e0145792. [PubMed: 26709830]

McKimpson WM, Zheng M, Chua SC, Pessin JE, and Kitsis RN (2017). ARC is essential for maintaining pancreatic islet structure and beta-cell viability during type 2 diabetes. Sci Rep 7, 7019. [PubMed: 28765602]

Medina-Ramirez CM, Goswami S, Smirnova T, Bamira D, Benson B, Ferrick N, Segall J, Pollard JW, and Kitsis RN (2011). Apoptosis inhibitor ARC promotes breast tumorigenesis, metastasis, and chemoresistance. Cancer Res 71, 7705–7715. [PubMed: 22037876]

Mercier I, Vuolo M, Jasmin JF, Medina CM, Williams M, Mariadason JM, Qian H, Xue X, Pestell RG, Lisanti MP, et al. (2008). ARC (apoptosis repressor with caspase recruitment domain) is a novel marker of human colon cancer. Cell Cycle 7, 1640–1647. [PubMed: 18469522]

Mercier I, Vuolo M, Madan R, Xue X, Levalley AJ, Ashton AW, Jasmin JF, Czaja MT, Lin EY, Armstrong RC, et al. (2005). ARC, an apoptosis suppressor limited to terminally differentiated

cells, is induced in human breast cancer and confers chemo- and radiation-resistance. Cell Death Differ 12, 682–686. [PubMed: 15861191]

Nam YJ, Mani K, Ashton AW, Peng CF, Krishnamurthy B, Hayakawa Y, Lee P, Korsmeyer SJ, and Kitsis RN (2004). Inhibition of both the extrinsic and intrinsic death pathways through nonhomotypic death-fold interactions. Mol Cell 15, 901–912. [PubMed: 15383280]

Nam YJ, Mani K, Wu L, Peng CF, Calvert JW, Foo RS, Krishnamurthy B, Miao W, Ashton AW, Lefer DJ, et al. (2007). The apoptosis inhibitor ARC undergoes ubiquitin-proteasomal-mediated degradation in response to death stimuli: identification of a degradation-resistant mutant. J Biol Chem 282, 5522–5528. [PubMed: 17142452]

Nikolova G, Jabs N, Konstantinova I, Domogatskaya A, Tryggvason K, Sorokin L, Fassler R, Gu G, Gerber HP, Ferrara N, et al. (2006). The vascular basement membrane: a niche for insulin gene expression and Beta cell proliferation. Dev Cell 10, 397–405. [PubMed: 16516842]

Otonkoski T, Banerjee M, Korsgren O, Thornell LE, and Virtanen I. (2008). Unique basement membrane structure of human pancreatic islets: implications for beta-cell growth and differentiation. Diabetes Obes Metab 10 Suppl 4, 119–127. [PubMed: 18834439]

Papa FR (2012). Endoplasmic reticulum stress, pancreatic beta-cell degeneration, and diabetes. Cold Spring Harb Perspect Med 2, a007666. [PubMed: 22951443]

Pick A, Clark J, Kubstrup C, Levisetti M, Pugh W, Bonner-Weir S, and Polonsky KS (1998). Role of apoptosis in failure of beta-cell mass compensation for insulin resistance and beta-cell defects in the male Zucker diabetic fatty rat. Diabetes 47, 358–364. [PubMed: 9519740]

Pop C, and Salvesen GS (2009). Human caspases: activation, specificity, and regulation. J Biol Chem 284, 21777–21781. [PubMed: 19473994]

Rhodes CJ (2005). Type 2 diabetes-a matter of beta-cell life and death? Science 307, 380–384. [PubMed: 15662003]

Rodriguez-Comas J, Moreno-Vedia J, Obach M, Castano C, de Pablo S, Alcarraz-Vizan G, Diaz-Catalan D, Mestre A, Horrillo R, Costa M, et al. (2020). Alpha1-antitrypsin ameliorates islet amyloid-induced glucose intolerance and beta-cell dysfunction. Mol Metab, 100984. [PubMed: 32229246]

Sandstrom CS, Ohlsson B, Melander O, Westin U, Mahadeva R, and Janciauskiene S. (2008). An association between Type 2 diabetes and alpha-antitrypsin deficiency. Diabet Med 25, 1370–1373. [PubMed: 19046232]

Stendahl JC, Kaufman DB, and Stupp SI (2009). Extracellular matrix in pancreatic islets: relevance to scaffold design and transplantation. Cell Transplant 18, 1–12. [PubMed: 19476204]

Stoss O, Schwaiger FW, Cooper TA, and Stamm S. (1999). Alternative splicing determines the intracellular localization of the novel nuclear protein Nop30 and its interaction with the splicing factor SRp30c. J Biol Chem 274, 10951–10962. [PubMed: 10196175]

Tabas I, and Ron D. (2011). Integrating the mechanisms of apoptosis induced by endoplasmic reticulum stress. Nat Cell Biol 13, 184–190. [PubMed: 21364565]

Tait SW, and Green DR (2010). Mitochondria and cell death: outer membrane permeabilization and beyond. Nat Rev Mol Cell Biol 11, 621–632. [PubMed: 20683470]

Talchai C, Xuan S, Lin HV, Sussel L, and Accili D. (2012). Pancreatic beta cell dedifferentiation as a mechanism of diabetic beta cell failure. Cell 150, 1223–1234. [PubMed: 22980982]

Templin AT, Samarasekera T, Meier DT, Hogan MF, Mellati M, Crow MT, Kitsis RN, Zraika S, Hull RL, and Kahn SE (2017). Apoptosis Repressor With Caspase Recruitment Domain Ameliorates Amyloid-Induced beta-Cell Apoptosis and JNK Pathway Activation. Diabetes 66, 2636–2645. [PubMed: 28729244]

Trapnell C, Roberts A, Goff L, Pertea G, Kim D, Kelley DR, Pimentel H, Salzberg SL, Rinn JL, and Pachter L. (2012). Differential gene and transcript expression analysis of RNA-seq experiments with TopHat and Cufflinks. Nature protocols 7, 562–578. [PubMed: 22383036]

Wang J, Takeuchi T, Tanaka S, Kubo SK, Kayo T, Lu D, Takata K, Koizumi A, and Izumi T. (1999). A mutation in the insulin 2 gene induces diabetes with severe pancreatic beta-cell dysfunction in the Mody mouse. J Clin Invest 103, 27–37. [PubMed: 9884331]

Wang M, Qanungo S, Crow MT, Watanabe M, and Nieminen AL (2005). Apoptosis repressor with caspase recruitment domain (ARC) is expressed in cancer cells and localizes to nuclei. FEBS Lett 579, 2411–2415. [PubMed: 15848180]

Weir GC, and Bonner-Weir S. (2004). Five stages of evolving beta-cell dysfunction during progression to diabetes. Diabetes 53 Suppl 3, S16–21. [PubMed: 15561905]

Wewers MD, Casolaro MA, Sellers SE, Swayze SC, McPhaul KM, Wittes JT, and Crystal RG (1987). Replacement therapy for alpha 1-antitrypsin deficiency associated with emphysema. N Engl J Med 316, 1055–1062. [PubMed: 3494198]

Yang WH, Park SY, Nam HW, Kim DH, Kang JG, Kang ES, Kim YS, Lee HC, Kim KS, and Cho JW (2008). NFkappaB activation is associated with its O-GlcNAcylation state under hyperglycemic conditions. Proc Natl Acad Sci U S A 105, 17345–17350. [PubMed: 18988733]

Yoshioka M, Kayo T, Ikeda T, and Koizumi A. (1997). A novel locus, Mody4, distal to D7Mit189 on chromosome 7 determines early-onset NIDDM in nonobese C57BL/6 (Akita) mutant mice. Diabetes 46, 887–894. [PubMed: 9133560]

Zaiman AL, Damico R, Thoms-Chesley A, Files DC, Kesari P, Johnston L, Swaim M, Mozammel S, Myers AC, Halushka M, et al. (2011). A critical role for the protein apoptosis repressor with caspase recruitment domain in hypoxia-induced pulmonary hypertension. Circulation 124, 2533–2542. [PubMed: 22082675]

Zhang B, Lu Y, Campbell-Thompson M, Spencer T, Wasserfall C, Atkinson M, and Song S. (2007). Alpha1-antitrypsin protects beta-cells from apoptosis. Diabetes 56, 1316–1323. [PubMed: 17360983]

Zhang K, and Kaufman RJ (2008). Identification and characterization of endoplasmic reticulum stress-induced apoptosis in vivo. Methods Enzymol 442, 395–419. [PubMed: 18662581]

Zhang Y, Proenca R, Maffei M, Barone M, Leopold L, and Friedman JM (1994). Positional cloning of the mouse obese gene and its human homologue. Nature 372, 425–432. [PubMed: 7984236]

Zhou YP, Pena JC, Roe MW, Mittal A, Levisetti M, Baldwin AC, Pugh W, Ostrega D, Ahmed N, Bindokas VP, et al. (2000). Overexpression of Bcl-x(L) in beta-cells prevents cell death but impairs mitochondrial signal for insulin secretion. Am J Physiol Endocrinol Metab 278, E340–351. [PubMed: 10662719]

Highlights

- Pancreatic β-cells unexpectedly synthesize and secrete the protease inhibitor AAT

- The cell death inhibitor ARC translocates to the nucleus of β-cells in diabetes

- Nuclear ARC downregulates AAT expression and secretion

- Loss of AAT disinhibits elastase causing β-cell detachment from matrix and cell death
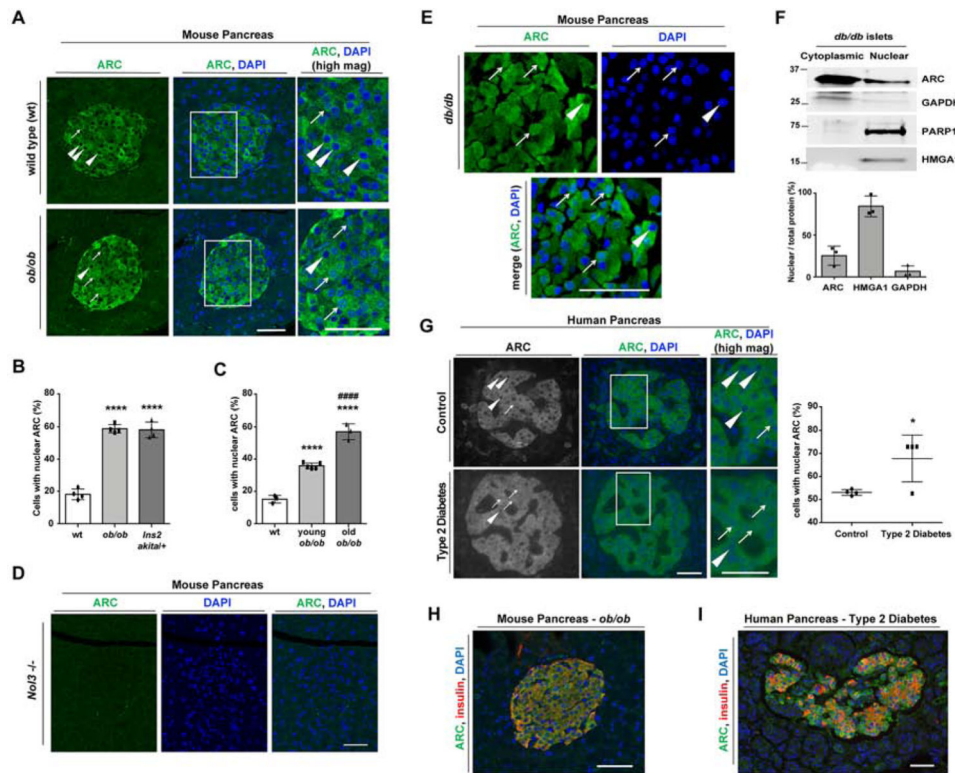
Figure 1. Translocation of ARC to the Nucleus of β-cells in Human and Mouse Diabetes
(A) ARC immunofluorescence of 20-week old male wild type (wt) and *ob/ob* mouse
pancreatic tissue imaged by confocal microscopy. Images on right are magnifications of
boxed areas. (B) Quantification of percentages of islet cells with nuclear ARC in wt, *ob/ob*,
and *Ins2* akita/+ mice. Each dot represents the mean of a sample from an independent
mouse. (C) Quantification of percentages of islet cells with nuclear ARC in wt, young (10-
week old) *ob/ob*, and old (20-week old) *ob/ob* mice. Each dot represents the mean of a
sample from an independent mouse. (D) ARC immunofluorescence in pancreatic tissue from
mice with homozygous deletion of *Nol3* encoding ARC showing no antibody reactivity. (E)
ARC immunofluorescence of 23-week old male *db/db* mouse pancreatic tissue imaged by
confocal microscopy. (F) Immunoblot (top) with quantification (bottom) of subcellular
fractionation of pancreatic islets isolated from *db/db* mice (16–18 weeks). GAPDH is
cytoplasmic marker; PARP1 and HMGA1 are nuclear markers. Each dot represents relative
protein abundance in islets isolated from an independent *db/db* mouse. (G) Left: ARC
immunofluorescence of human pancreatic tissue from individuals with and without type 2
diabetes (see Table S1). Black and white images of ARC staining alone (left), pseudocolored
images of ARC merged with DAPI (center), and higher power (high mag) view of boxed
areas (right). Right: Quantification of islet cells with nuclear ARC. Each dot represents the
mean for an individual person. Group means are demarcated by the horizontal bars. (H) and
(I) Immunostaining for ARC (green) and β-cell marker insulin (red) in mouse (panel H) and
human (panel I) pancreatic tissue. Individual channels are shown in Figure S2. Nuclei
counterstained with DAPI. Scale bars 50 μM. Confocal images were scanned with pinhole
size of 1 airy unit. White arrow denotes representative cell with colocalization of nuclear

ARC (green) and DAPI (blue). Arrowhead denotes representative cell with no overlap of ARC and DAPI. Data are presented as mean ± SD. Comparisons between two groups were made using a two-tailed student's t-test and among multiple groups using analysis of variance followed by a Tukey post-hoc test. * P < 0.05. **** P < 0.0001 versus wt and #### P < 0.0001 versus young *ob/ob*.
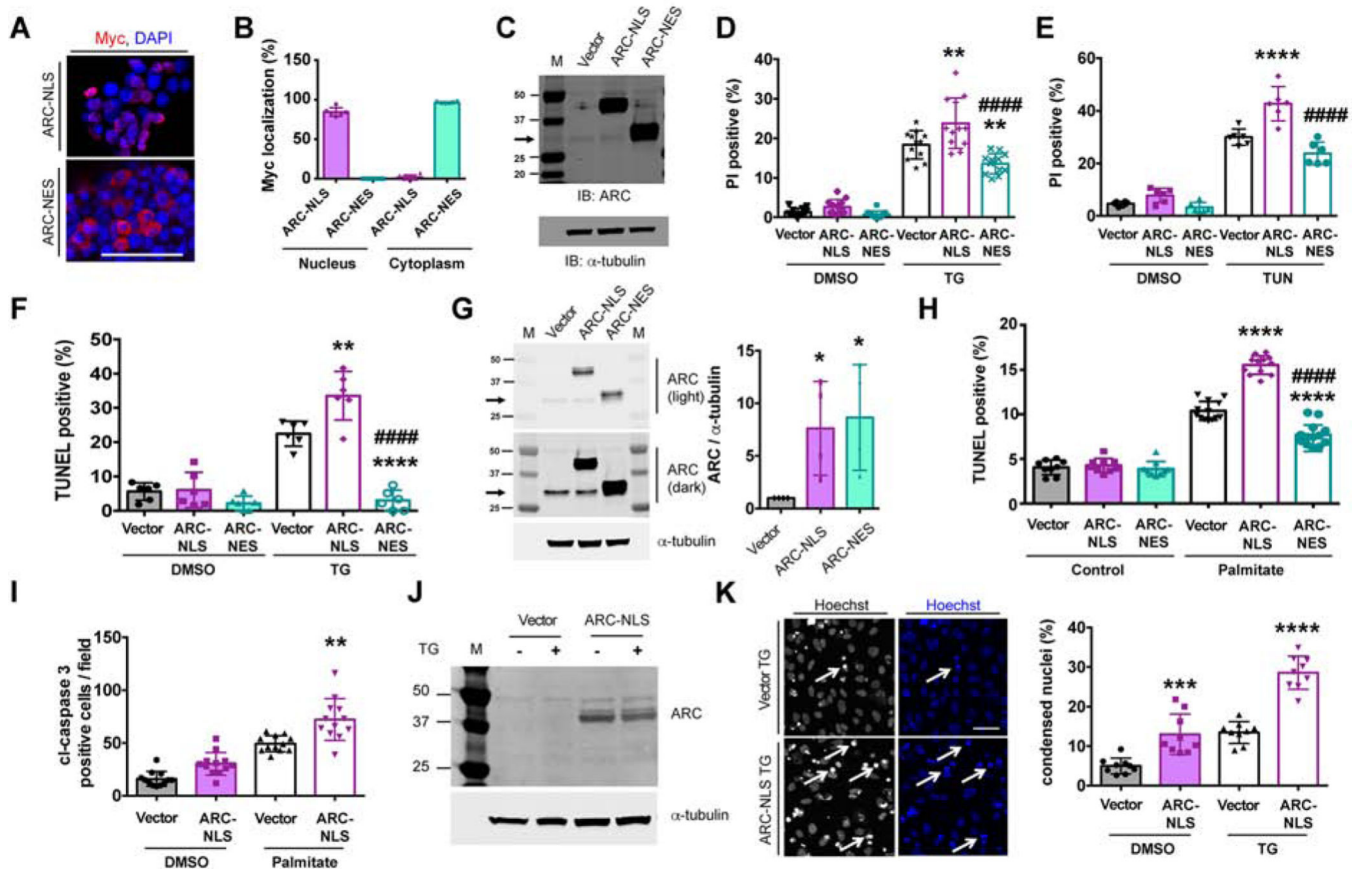
Figure 2. Nuclear ARC Exacerbates ER Stress-induced β-cell Death

(A) Confocal images of immunofluorescence of Myc-tagged ARC-NLS and ARC-NES transiently transfected into MIN6 β-cells. Scale bar 50 μM. (B) Quantification of data from panel A. Individual dots denote technical replicates. (C) Immunoblot for ARC in MIN6 cell lysates following transient transfection of empty vector, ARC-NLS, or ARC-NES. Arrow demarcates endogenous ARC. (D and E) Cell death as scored by propidium iodide (PI) staining following overnight treatment with 1 μM thapsigargin (TG, panel D) or 5 ng/mL tunicamycin (Tun, panel E) of MIN6 cells transiently transfected with vector, ARC-NLS, or ARC-NES. (F) Apoptosis as assessed by TUNEL following TG treatment of MIN6 cells transiently transfected with vector, ARC-NLS, or ARC-NES. (G) Immunoblot for ARC in lysates of MIN6 cells stably transfected with vector, ARC-NLS, and ARC-NES. Arrow demarcates endogenous ARC (left). Quantification of independent experiments (right). (H and I) Cell death as assessed by TUNEL (panel H) or cleaved (cl) caspase-3 (panel I) of MIN6 cells stably transfected with vector, ARC-NLS, or ARC-NES and then treated overnight with 1.2 mM palmitate. (J) Immunoblot for ARC in lysates of U2OS cells (lacking endogeneous ARC) transiently transfected with vector or ARC-NLS and then treated with DMSO (−) or TG (+). (K) Apoptosis as assessed by nuclear condensation of Hoechst 33342-stained U2OS cells transiently transfected with vector or ARC-NLS and then treated with DMSO or TG. Confocal black and white images (left) and pseudocolored images (right) of Hoechst are displayed. White arrows denote condensed nuclei. Scale bar 50 μM. Confocal images were scanned with pinhole size of 1 airy unit. All panels, except panels D, E, and F,

represent pooled data from ≥3 independent experiments. Due to technical variation in the magnitude of the death stimulus, replicates from a single experiment are displayed in panels D, E, and F to show the actual experimental values. For these panels, pooled data with values normalized from ≥3 independent experiments are displayed in Figure S3. It is important to note that while absolute numbers of apoptotic cells varied between replicates, relative differences in ARC-NLS exacerbation (and ARC-NES protection) from death stimuli were similar in all experiments. All data are presented as mean ± SD. Differences among multiple groups were analyzed using analysis of variance followed by a Tukey post-hoc test. * $P < 0.05$, ** $P < 0.01$, *** $P < 0.001$, **** $P < 0.0001$ for ARC-NLS or ARC-NES compared with vector. #### $P < 0.0001$ for ARC-NLS compared with ARC-NES. Not shown: $P < 0.0001$ for thapsigargin, tunicamycin, and palmitate versus control treatments for vector and ARC-NLS cells (all panels) and for ARC-NES (panels D, E, and H).
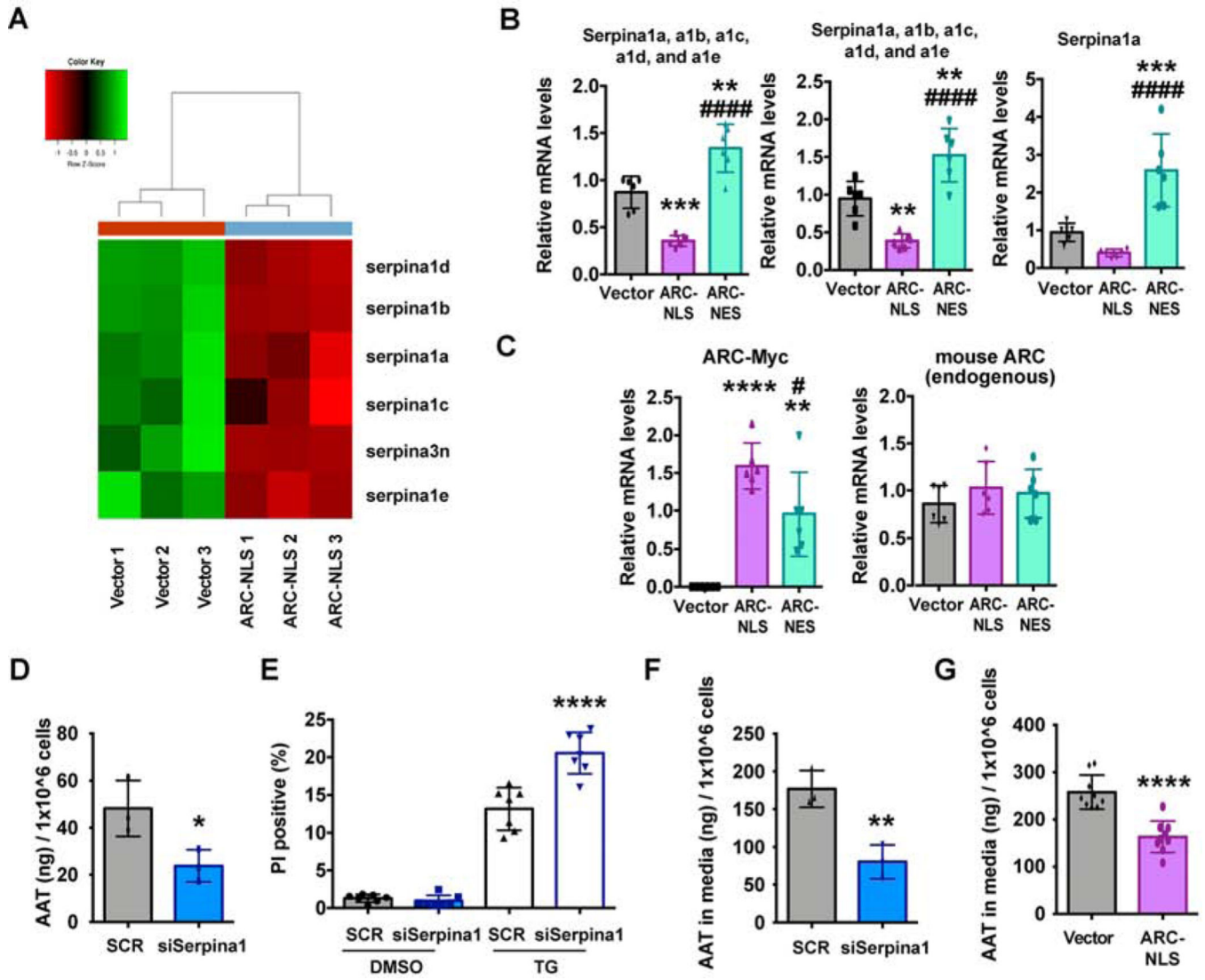
Figure 3. Nuclear ARC Decreases Expression of Multiple Serpin Genes

(A) Heat map of differentially abundant serpin transcripts resulting from RNA-seq analysis of MIN6 cells with stable transfection of ARC-NLS as compared with vector. (B) qRT-PCR confirmation of changes in abundance of serpin transcripts in MIN6 stably transfected with ARC-NLS, ARC-NES, or vector. Primer pairs in the left and middle graphs assess transcripts from *serpina1a*, *a1b*, *a1c*, *a1d*, and *a1e*, while those on the far right assess transcripts only from *serpina1a*. (C) Left: qRT-PCR confirmation that human ARC is overexpressed in MIN6 cells stably transfected with ARC-NLS and ARC-NES as compared with vector. As per Methods, primer pair designed to recognize only overexpressed construct and not endogenous ARC. Right: qRT-PCR confirmation that endogenous ARC mRNA levels (recognized by primers specific to mouse ARC) remained unchanged when ARC-NLS, ARC-NES, and vector are overexpressed. (D) ELISA for SERPINA1 (α_1-antitrypsin or AAT, the single protein encoded by serpins a1a, a1b, a1c, a1d, and a1e) in lysates of MIN6 cells transfected with scrambled (SCR) siRNA or siRNA (siSerpina1) directed against *serpina1a*, *a1b*, and *a1c* mRNAs. (E) Cell death as assessed by PI staining in MIN6 cells

transfected with SCR or siSerpina1 siRNA and then treated overnight with DMSO or 1 μM thapsigargin (TG). (F) ELISA for AAT in media from cultures of MIN6 cells transfected with SCR or siSerpina1 siRNA. (G) ELISA for AAT in media from cultures of MIN6 cells with stable transfection of vector or ARC-NLS. Data are presented as mean ± SD. The RNA-seq analysis was performed once with 3 technical replicates in each group. Data in other panels are from independent experiments with N = 2 in panels B and C and N ≥ 3 in the panels D-G. Comparisons between two groups were made using a two-tailed student's t-test and among multiple groups using analysis of variance followed by a Tukey post-hoc test. * P < 0.05, ** P < 0.01, *** P < 0.001, **** P < 0.0001 for ARC-NLS, ARC-NES, or siSerpina1 compared with vector or control SCR siRNA. # P < 0.05, #### P < 0.0001 for ARC-NES compared with ARC-NLS. Not shown: P < 0.0001 for thapsigargin versus control treatment for SCR and siSerpina1 cells.
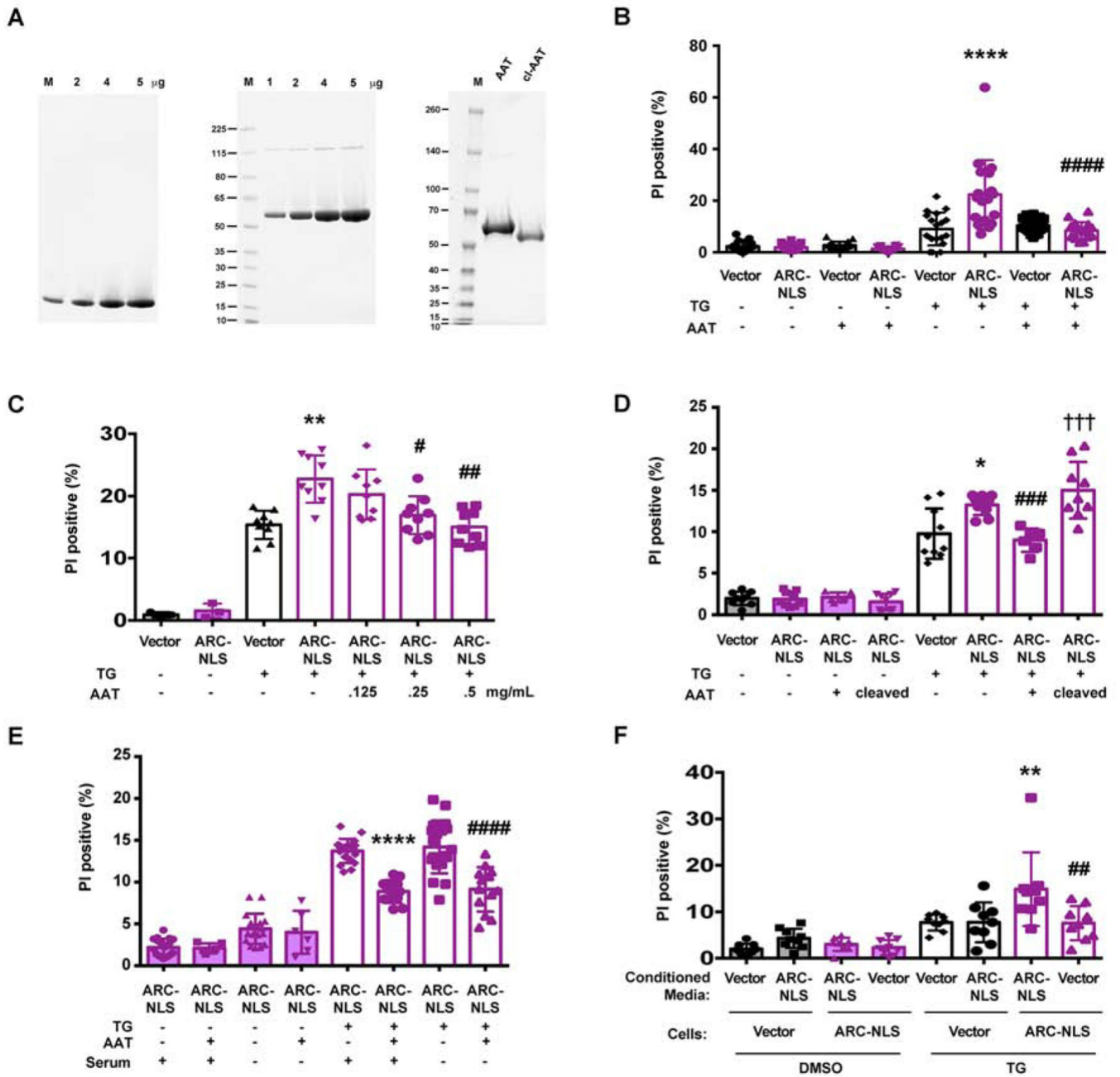
Figure 4. Extracellular AAT can Rescue ARC-NLS Induced Cell Death

(A) Coomassie blue-stained PAGE analysis of AAT purified from human plasma. Left gel: 3–12% Bis-Tris native gel showing increasing amounts of intact AAT. Middle gel: 412% Bis-Tris Nu PAGE (denaturing gel) showing increasing amounts of intact AAT. Right gel: 4–12% Bis-Tris Nu PAGE (denaturing gel) comparing intact AAT and AAT cleaved with endoproteinase GluC followed by chromatography to remove the GluC. (B) Cell death as assessed by PI staining in MIN6 cells with stable transfection of vector or ARC-NLS and then treated overnight with DMSO or 1 μM TG. Where indicated, purified human AAT (0.5 mg/ml) was added to the cell culture media prior to treatment. (C) - (E) Experiments

analogous to panel B. Purified human AAT of varying concentrations was added to the cell culture media (panel C), intact or cleaved human AAT was added to the cell culture media (panel D), or purified human AAT (0.5 mg/ml) was added to media in the presence or absence of serum (panel E). (F) Cell death as assessed by PI staining in MIN6 cells stably transfected with vector or ARC-NLS that have been cultured in media conditioned by MIN6 cells stably transfected with vector or ARC-NLS following which they were treated by DMSO or TG. Data are presented as mean ± SD. Each panel, except Panel F, is representative experiment of 3 independent experiments. For Panel F, one experiment is displayed to show actual magnitude of effects and pooled data, with values normalized to treatment, from 3 independent experiments is displayed in Figure S5. It is important to note that while absolute numbers of apoptotic cells varied between replicates in panel F, relative differences in ARC-NLS exacerbation of cell death (and protection with vector media) were similar in all experiments. Differences among multiple groups were analyzed using analysis of variance followed by a Tukey post-hoc test. * $P < 0.05$, ** $P < 0.01$, **** $P < 0.0001$ for ARC-NLS TG compared with vector TG. # $P < 0.05$, ## $P < 0.01$, ### $P < 0.001$, #### $P < 0.0001$ for effects of AAT and conditioned media. ††† $P < 0.001$ for cleaved versus intact AAT. Not shown are comparison between thapsigargin versus control treatments: panel B: vector $P < 0.01$, ARC-NLS $P < 0.0001$, vector + AAT $P < 0.01$, ARC-NLS + AAT $P < 0.01$; panels C-E: $P < 0.0001$; panel F: vector cells/vector media $P < 0.05$ and ARC-NLS cells/ARC-NLS media $P < 0.0001$.
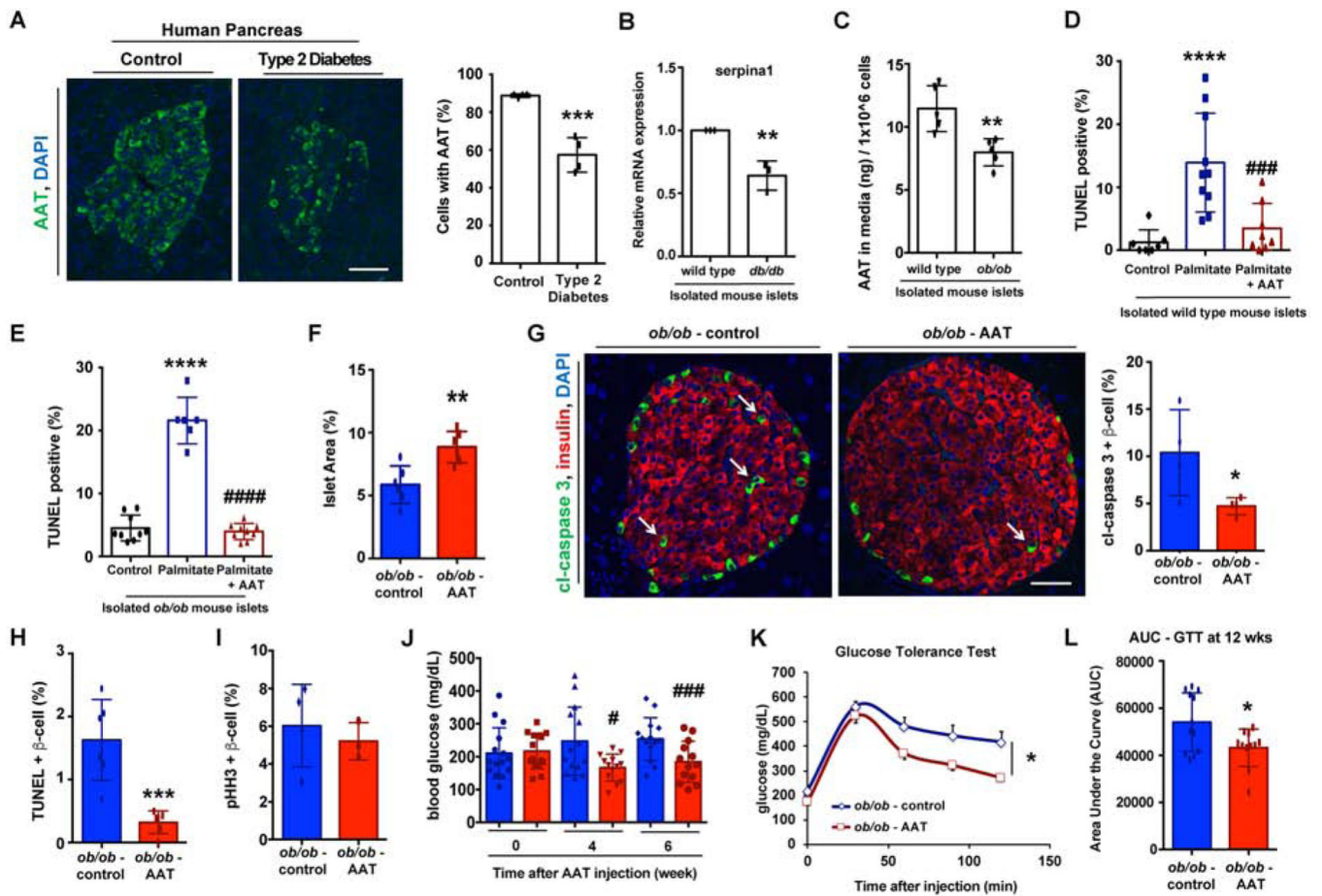
Figure 5. Administration of AAT Prevents β-cell Death and Progression of Diabetes in *ob/ob* Mice

(A) AAT immunofluorescence (left) with quantification (right) of human pancreatic tissue from individuals with and without type 2 diabetes (Table S1). Nuclei are counterstained with DAPI. Each dot represents an individual. *** P < 0.001. Scale bar 50 μM. (B) qPCR measurements of *serpina1* gene expression in islets isolated from 23-week old male wild type and *db/db* mice. Each dot represents an independent islet preparation. ** P < 0.01. (C) ELISA for SERPINA1 (α_1-antitrypsin or AAT, the single protein encoded by serpins a1a, a1b, a1c, a1d, and a1e) in media from cultures of islets isolated from 12-week old wild type and *ob/ob* mice. Each dot represents an independent islet preparation. ** P < 0.01. (D) and (E) Cell death as assessed by TUNEL staining in islets isolated from 12-week old wild type (panel D) and *ob/ob* (panel E) mice after treatment with palmitate (1.2mM for 3 days). Where indicated, purified human AAT (0.5 mg/ml) was added to the islet culture media prior to treatment. Data from 3 independent islet preprations with dots showing all technical replicates. **** P < 0.0001 for effects of treatment. ### P < 0.001, #### P < 0.0001 for effects of AAT. (F) – (L) Male *ob/ob* mice were randomized to receive AAT (2 mg/mouse in water; see Methods for details) or water alone by intraperitoneal injection every 3 days starting at 9-weeks of age and continuing for 14 weeks. N = 15 mice/group at start of experiment. Over the 14-week treatment protocol, 3 mice in the control group and 4 mice in the AAT group died. Each dot represents an individual randomly chosen mouse. Solid blue

bar denotes control group and red bar denotes AAT group. (F) Quantification of pancreatic islet area after 14 weeks of AAT treatment. ** $P < 0.01$. (G) Cleaved (cl) caspase 3 (green) staining (left) with quantification (right) of pancreatic tissue after 14 weeks of treatment. Insulin (red) demarcates β-cells and DAPI counterstains nuclei. White arrows denote cl-caspase 3-positive β-cell. Scale bar 50 μM. * $P < 0.05$. (H) Quantification of β-cell death using TUNEL staining, a second marker of apoptosis. Representative images are displayed in Figure S6. *** $P < 0.001$. (I) Quantification of β-cell proliferation using phospho-histone H3 (pHH3) staining showing no significant differences. (J) Fasting blood glucose concentrations at times indicated. # $P < 0.05$ at 4 weeks of treatment. ### $P < 0.001$ at 6 weeks of treatment. (K) Glucose tolerance test (GTT) at 12-weeks of treatment. (L) Area under the curve (AUC) calculations for the GTT displayed in panel K. * $P < 0.05$. Data are presented as mean ± SD. Statistics are shown for each panel with comparisons between two groups made using a two-tailed student's t-test and among multiple groups using analysis of variance followed by a Tukey post-hoc test.
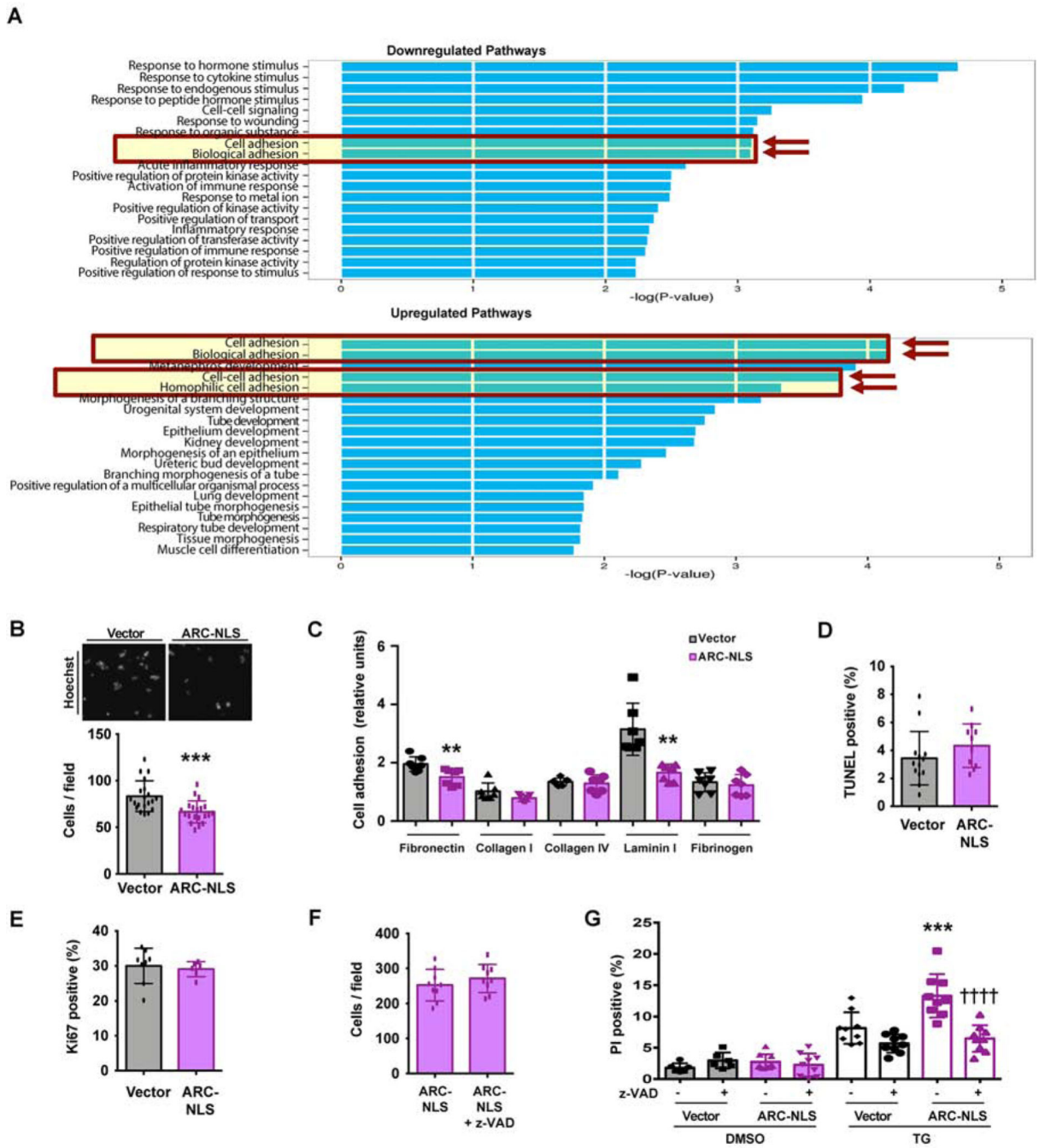
Figure 6. Nuclear ARC Disrupts Cell Adhesion

(A) Gene ontology analysis of cells. This analysis is based on RNA-seq data comparing MIN6 cells with stable transfection of ARC-NLS versus empty vector. Statistically significant pathways altered by nuclear ARC are shown (P < 0.01). Arrows with shaded boxes demarcate pathways involved in cell adhesion. (B) Adhesion to tissue culture plates of MIN6 cells with stable transfection of vector or ARC-NLS as visualized by Hoechst 33342 staining. (C) Relative adhesion of MIN6 cells with stable transfection of vector or ARC-NLS to tissue culture plates coated with various extracellular matrix proteins. (D) and (E)

Changes in cell death (TUNEL, panel D) and proliferation (Ki67, panel E) were not observed over the time course of the adhesion experiments. (F) Adhesion to tissue culture plates of MIN6 cells stably transfected with ARC-NLS in the presence or absence of 200 μM z-VADfmk (z-VAD), a pan-caspase inhibitor. z-VAD was added after overnight plating and the experiment continued for an additional 24 h. (G) Cell death as assessed with PI staining of MIN6 cells stably transfected with vector or ARC-NLS following overnight treatment with DMSO or 1 μM thapsigargin (TG). Where indicated, cells were pre-treated for 2h with z-VAD to block thapsigargin-induced cell death. Unless otherwise indicated, experiments were performed on uncoated tissue culture plates. Data are presented as mean ± SD. Data shown in each panel are 3 independent experiments with the exception of the RNA-seq analysis which was performed once with 3 technical replicates in each group. Comparisons between two groups made using a two-tailed student's t-test and among multiple groups using analysis of variance followed by a Tukey post-hoc test. ** P < 0.01, *** P < 0.001 for ARC-NLS compared with corresponding control vector. †††† P < 0.0001 compared with no z-VAD. Not shown are comparison between thapsigargin versus control treatments: vector P < 0.0001, ARC-NLS P < 0.0001, ARC-NLS + z-VAD P < 0.01.
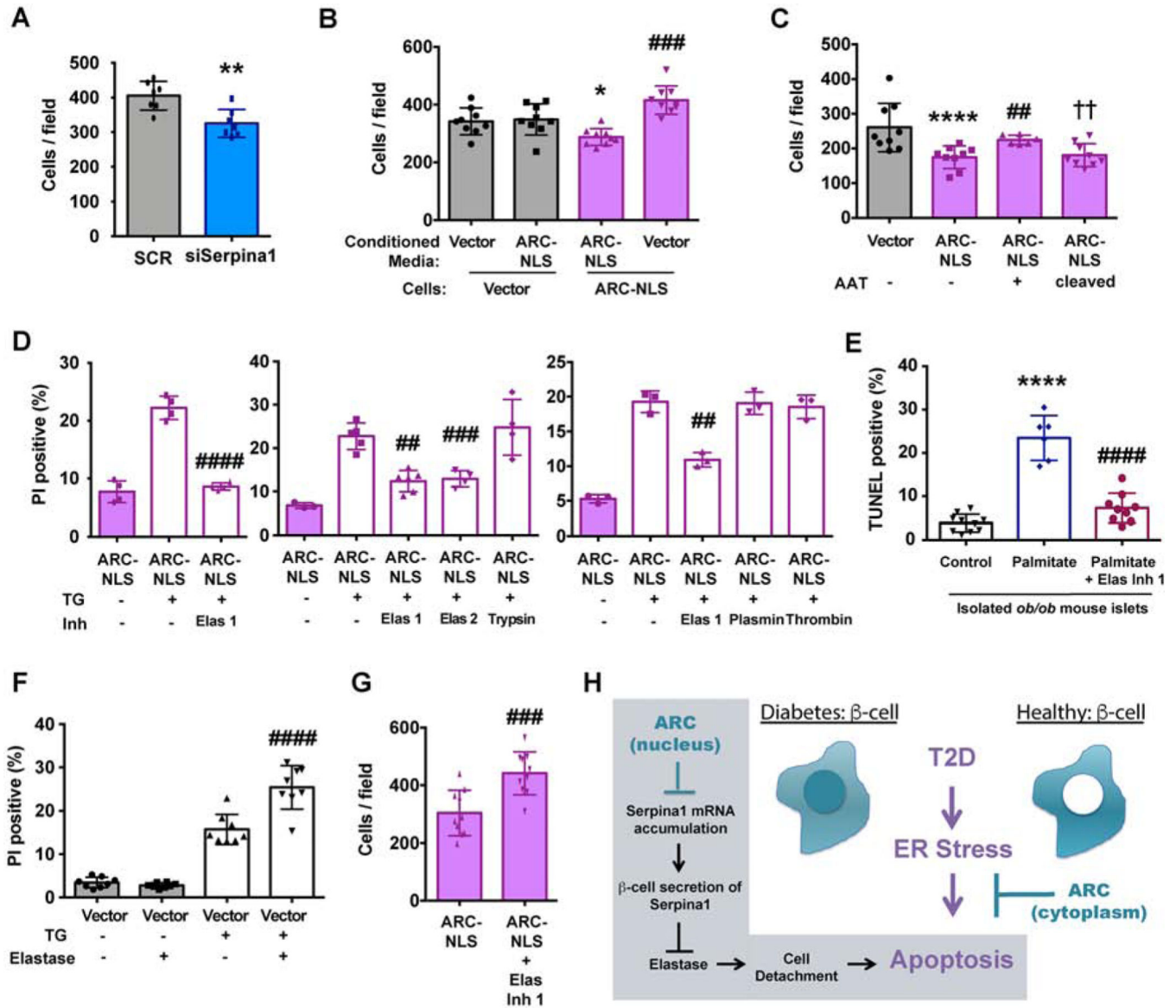
Figure 7. Loss of Extracellular AAT Triggers Elastase-dependent Disruption of Cell Adhesion and Cell Death

(A) Adhesion to tissue culture dishes of MIN6 cells transfected with SCR or siSerpina1 siRNA. (B) Adhesion to tissue culture plates of MIN6 cells with stable transfection of vector or ARC-NLS in the presence of media conditioned by MIN6 cells transfected with vector or ARC-NLS. (C) Adhesion to tissue culture plates of MIN6 cells with stable transfection of ARC-NLS in the presence or absence of intact or cleaved AAT (0.5 mg/ml). (D) Cell death as assessed by PI staining in MIN6 cells stably transfected with ARC-NLS which were pre-incubated with the indicated inhibitors (Inh), including elastase inhibitors *N*-methoxysuccinyl-Ala-Ala-Pro-Val-chloromethyl ketone (Elas Inh 1; 0.2 mg/mL) and the recombinant protein elafin (Elas Inh 2; 0.1 mg/mL), following which they were treated overnight with 1 μM thapsigargin (TG). (E) Cell death as assessed by TUNEL staining in islets isolated from 12-week old *ob/ob* mice after treatment with palmitate (1.2mM for 3

days). Where indicated, Elas Inh 1 was added to the islet culture media prior to treatment. (F) Cell death as assessed by PI staining in MIN6 cells stably transfected with vector which were incubated with purified elastase following which they were treated with TG. (G) Adhesion to tissue culture plates of MIN6 cells with stable transfection of ARC-NLS in the presence of the Elas Inh 1. (H) Model by which cytoplasmic ARC promotes β-cell survival and nuclear ARC potentiates β-cell death. Data are presented as mean ± SD. Panels A, C, and E show data from 3 independent experiments, and panels F and G from 2 independent experiments. Panel B is a representative experiment to show the absolute values, with normalized pooled data from 3 independent experiments in Figure S5. Panel D shows three independent experiments. Comparisons between two groups made using a two-tailed student's t-test and among multiple groups using analysis of variance followed by a Tukey post-hoc test. * $P < 0.05$, ** $P < 0.01$, **** $P < 0.0001$ for Serpina1 siRNA, ARC-NLS, or palmitate treatment compared with corresponding SCR siRNA, control vector, or control media respectively. ## $P < 0.01$, ### $P < 0.001$, #### $P < 0.0001$ for effects of conditioned media, AAT, elastase, and inhibitors. †† $P < 0.01$ for cleaved versus intact AAT. Not shown: $P < 0.0001$ for thapsigargin versus control and thapsigargin + elastase versus elastase treatments.

KEY RESOURCES TABLE

REAGENT or RESOURCE	SOURCE	IDENTIFIER
Antibodies		
ARC (recognizes the C-terminus of both human and mouse ARC)	Cayman Chemical	cat# 160737, RRID:AB_10079432
α-tubulin	Sigma-Aldrich	cat# T9026, RRID:AB_477593
Insulin	Abcam	cat# ab7842, RRID:AB_306130
Insulin	Dako	cat# A056401-2 RRID:AB_2617169
AAT	provided by E. Miranda, Sapienza University of Rome and J. Perez, University of Malaga	n/a
Ki67	Abcam	cat# ab15580, RRID:AB_443209
Cleaved caspase-3 (Asp175)	Cell Signaling Technology	cat# 9661, RRID:AB_2341188
Myc-Tag (9B11)	Cell Signaling	cat# 2276S, RRID:AB_331783
Anti-Histone H3 (phospho S10)	Abcam	cat# ab5176 RRID:AB_304763
GAPDH (EPR16891)	Abcam	cat# ab181602 RRID:AB_2630358
HMGA1 (EPR7839)	Abcam	cat# ab129153 RRID:AB_11139631
PARP1 (CL2220)	Sigma-Aldrich	cat# AMAB90959 RRID:AB_2665732
IRDye 800CW	LI-COR	cat# 926-32212 (RRID:AB_621847) and 926-32213 (RRID:AB_621848)
IRDye 680RD	LI-COR	cat# 926-68073 (RRID:AB_10954442) and 926-68072 (RRID:AB_10953628)
Alexa Fluor 488	Invitrogen	cat# A-11029 (RRID:AB_138404) and A-11034 (RRID:AB_2576217)
Alexa Fluor 568	Invitrogen	cat# A-11031 (RRID:AB_144696) and A-11036 (RRID:AB_143011)
Alexa Fluor 647	Invitrogen	cat# A-21450 (RRID:AB_141882)
Bacterial and Virus Strains		
Biological Samples		
Human tissue samples	Network for Pancreatic Organ Donors with Diabetes (nPOD)	See supplemental table in paper
Chemicals, Peptides, and Recombinant Proteins		
AAT (cell treatments)	Sigma-Aldrich and purified in laboratory	cat# SRP6312-1MG
Cleaved-AAT	Generated/purified in laboratory	n/a
AAT (Prolastin C; mouse injections)	Obtained directly from Grifols	n/a
Hoechst 33342	Invitrogen	cat# H3570
Tunicamycin	Sigma-Aldrich	cat# T7765-1MG
Thapsigargin	Fisher Scientific	cat# T7458
Palmitate	Sigma-Aldrich	cat# P9767-5G
Propidium iodide	Sigma-Aldrich	cat# P4170-25MG
z-VADfmk	R&D Systems	cat# FMK001

REAGENT or RESOURCE	SOURCE	IDENTIFIER
N-methoxysuccinyl-Ala-Ala-Pro-Val-chloromethyl ketone	Sigma-Aldrich	cat# M0398-5MG
elafin	Sigma-Aldrich	cat# E7280-100UG
BPTI	Sigma-Aldrich	cat# 10236624001
Thrombin Inhibitor	SensoLyte AFC kit by AnaSpec	cat# AS-72129
Trypsin inhibitor	Sigma-Aldrich	cat# T0256-1MG
Elastase	SensoLyte AFC kit by AnaSpec	cat# AS-72179
Critical Commercial Assays		
Fluorescein In Situ Cell Death Detection Kit	Roche Applied Science	cat# 11684795910
CytoSelect 48-Well Cell Adhesion Assay ECM Array	Cell Biolabs	cat# CBA-070
SERPINA1 ELISA Kit (serpin Peptidase Inhibitor, Clade A (Alpha-1 Antiproteinase, Antitrypsin), Member 1)	Abnova	cat# ABIN424274
Arcturus PicoPure RNA Isolation Kit	Applied Biosystems	cat# KIT0204
qScript cDNA SuperMix	Quanta Biosciences	cat# 95048-025
GoTaq qPCR Master Mix	Promega	cat# A6001
Cell Fractionation Kit	Thermo Fisher	cat# 78833
Deposited Data		
ARC-NLS RNA-seq	Generated for paper	SRA accession: PRJNA563773; https://www.ncbi.nlm.nih.gov/sra/PRJNA563773
Experimental Models: Cell Lines		
MIN6 cells	Provided from Peter Arvan at the University of Michigan	n/a
U2OS cells	ATCC	cat# ATCC HTB-96 (RRID:CVCL_0042)
Experimental Models: Organisms/Strains		
Leptin *ob/ob* mice	Jackson Laboratory	cat# 000632 (RRID:IMSR_JAX:000632)
Ins2 Akita mice	Jackson Laboratory	cat# 003548 (RRID:IMSR_JAX:003548)
db/db mice	Jackson Laboratory	cat# 000697 (RRID:IMSR_JAX:000697)
Wildtype (c57bl/6) mice	Generated from breeding mouse lines above	
Nol3 –/– mice	(Medina-Ramirez et al., 2011; Zaiman et al., 2011)	n/a
Oligonucleotides		
ARC-Myc (to detect ARC-NLS and ARC-NES constructs) primer sequence: Forward: 5'-TGGAAGCTGAGGCCTCTAAA-3' (recognizes only human ARC); Reverse: 5'-GCCCCATTCAGATCCTCTT-3' (recognizes Myc tag)	Generated for paper	n/a
Mouse ARC (endogenous ARC in MIN6 cells) primer sequence: Forward: 5'- CAAGAAGAGGATGAATCTGAAG-3'; Reverse: 5'- TTGGCAGTAGGTGTCTCG-3'	Generated for paper	n/a
Serpina1a, a1b, a1c, a1d, a1e primer #1 sequence: Forward: 5'- TAGGGAGCAAGGGTGACACTC-3'; Reverse: 5'- ACTGTCTGGTCTGTTGAGGGT-3'	from MGH PrimerBank (serpina1e)	https://pga.mgh.harvard.edu/cgi-bin/primerbank/new_search2.cgi

REAGENT or RESOURCE	SOURCE	IDENTIFIER
Serpina1a, a1b, a1c, a1d, a1e primer #2 sequence: Forward: 5'-TTCCAACACCTCCTCCAAAC-3'; Reverse: 5'-CACTTTCTTGGCCTCCTCTG-3'	Generated for paper	n/a
Serpina1a primer sequence: Forward: 5'-TGCCTGATGCTACAGCAAGT-3'; Reverse: 5'-AACCTATTTGCATGGCTGGA-3'	Generated for paper	n/a
CHOP primer sequence: Forward: 5'-CTGCCTTTCACCTTGGAGAC-3'; Reverse: 5'-CGTTTCCTGGGGATGAGATA-3'	(Zhang and Kaufman, 2008)	n/a
GAPDH primer sequence: Forward: 5'-CGTATTGGGCGCCTGGTCAC-3'; Reverse: 5'-ATGATGACCCTTTTGGCTCC-3'	Generated for paper	n/a
Serpin siRNA	Life Technologies	cat# s74223
SCR siRNA	Life Technologies; Silencer™ Select Negative Control No. 1 siRNA	cat# 4390843
Recombinant DNA		
ARC-NLS	Generated for studies in this paper	Will be provided on request
ARC-NES	Generated for studies in this paper	Will be provided on request
Software and Algorithms		
GraphPad Prism 6	GraphPad Software	
ImageJ	NIH	https://imagej.nih.gov/ij/
Tophat version 2.0.11	(Trapnell et al., 2012)	
Cufflinks version 2.2.1	(Trapnell et al., 2012)	
Cuffdiff version 2.2.1	(Trapnell et al., 2012)	
UCSC Genome Browser	(Kent et al., 2002)	
Database for Annotation, Visualization and Integrated Discovery	(Huang da et al., 2009)	http://david.abcc.ncifcrf.gov/
Other		